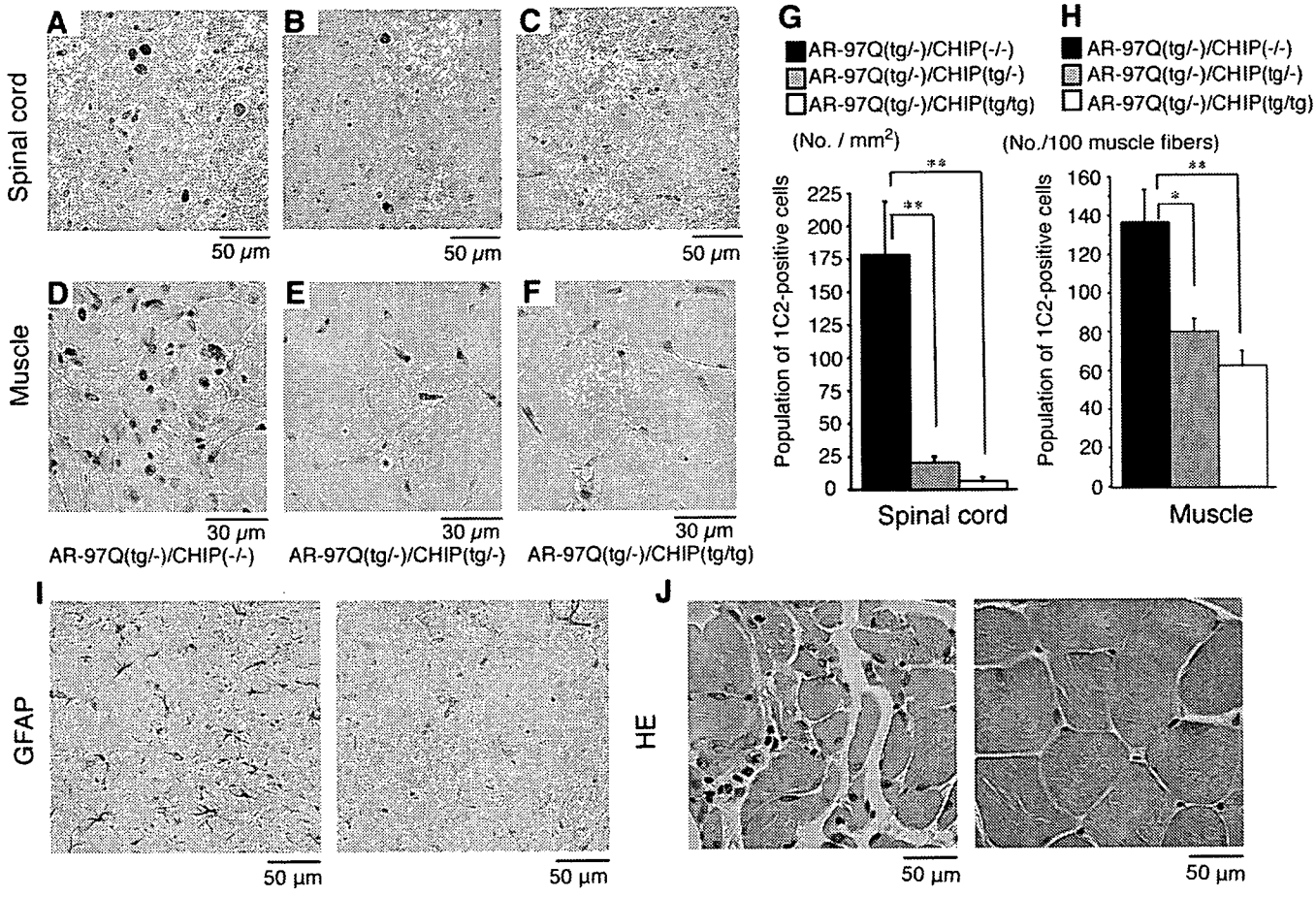

Figure 5. CHIP decreases nuclear-localized mutant AR in double-transgenic mice. ***A–F***, PolyQ immunohistochemistry (1C2) in the spinal anterior horn (***A–C***) and muscle (***D–F***) of 16-week-old AR-97Q/CHIP$^{(-/-)}$ and AR-97Q/CHIP double-transgenic mice. AR-97Q/CHIP$^{(-/-)}$ mice have intense and frequent staining for 1C2 in the nucleus (***A***, ***D***). ***B***, ***C***, ***E***, ***F***, AR-97Q/CHIP$^{(tg/-)}$ (***B***, ***E***) and AR-97Q/CHIP$^{(tg/tg)}$ (***C***, ***F***) mice exhibit low levels of 1C2 staining in the nucleus. ***G***, ***H***, Quantitative assessment of diffuse nuclear staining for 1C2 in the spinal ventral horn (***G***) and muscle (***H***). Bars represent the density of 1C2-positive cells in the AR-97Q/CHIP$^{(-/-)}$, AR-97Q/CHIP$^{(tg/-)}$, and AR-97Q/CHIP$^{(tg/tg)}$ mice. There are significantly more 1C2-positive cells in AR-97Q/CHIP$^{(-/-)}$ mice than in AR-97Q/CHIP$^{(tg/-)}$ mice or AR-97Q/CHIP$^{(tg/tg)}$ mice in both tissues. Results are expressed as mean ± SEM for six mice. *$p < 0.025$; **$p < 0.005$. ***I***, Immunohistochemical staining with GFAP-specific antibody also showed an obvious reduction in reactive astrogliosis in the spinal anterior horn of AR-97Q/CHIP$^{(tg/tg)}$ mice. ***J***, Hematoxylin and eosin (HE) staining of muscle tissue in AR-97Q/CHIP$^{(-/-)}$ mice revealed obvious atrophy and small-angulated fibers, which were not seen in AR-97Q/CHIP$^{(tg/tg)}$ mice. No., Number.

AR-97Q/CHIP double-transgenic mice. More importantly, CHIP also colocalized with mutant AR aggregates present in the anterior horn cells from postmortem tissues of SBMA patients. Western blot analysis showed that both a band of monomeric mutant AR and the high-molecular-weight form of mutant AR protein complexes retained in the stacking gel were diminished in the spinal cord and muscle of the double-transgenic mice, suggesting that the degradation of mutant AR may have been accelerated by overexpression of CHIP.

Our AR-97Q transgenic mice display progressive muscular atrophy and weakness, as well as diffuse nuclear staining and NIs of the mutant AR (Katsuno et al., 2002). These phenotypes are very pronounced in male transgenic mice, similar to human SBMA patients. The fact that AR has a specific ligand (i.e., testosterone), renders the pathogenesis of SBMA unique among polyQ diseases (Poletti et al., 2005). There is increasing evidence that the AR ligand (Katsuno et al., 2003; Chevalier-Larsen et al., 2004; Sopher et al., 2004; Katsuno et al., 2006; Yu et al., 2006) and molecular chaperones (Kobayashi et al., 2000; Bailey et al., 2002; Adachi et al., 2003) play a crucial role in the pathogenesis of SBMA. The success of androgen deprivation therapy in SBMA mouse models has been translated into clinical trials (Banno et al., 2006). In addition, elucidation of its pathophysiology using SBMA animal models has led to the development of other chaperone-related disease-modifying drugs, an Hsp90 inhibitor (Waza et al., 2005) and a heat shock protein inducer (Katsuno et al., 2005), which inhibit the pathogenic process of neuronal degeneration. Recent studies suggested that soluble causative protein species, not insoluble protein aggregates, might be toxic and thus targets in treatments of neurodegenerative disorders (Slow et al., 2006). Here, we demonstrated that overexpression of human CHIP exerts therapeutic effects on motor dysfunction in the AR-97Q mouse. Overexpression of CHIP served to decrease monomeric mutant AR in the double-transgenic mice. The large aggregated mutant AR protein complexes were also significantly reduced by CHIP overexpression, suggesting that CHIP accelerated the turnover of mutant AR. Together, these data suggest that targeting mutant AR for proteasomal degradation by overexpression of CHIP could be a disease-modifying therapeutic strategy in SBMA neuropathology. These findings are consistent with previous studies showing that CHIP serves as a protective factor in other polyQ diseases by promoting reduced aggregation of disease proteins (Jana et al., 2005; Miller et al., 2005) and proteasomal degradation (Al-Ramahi et al., 2006). In contrast to

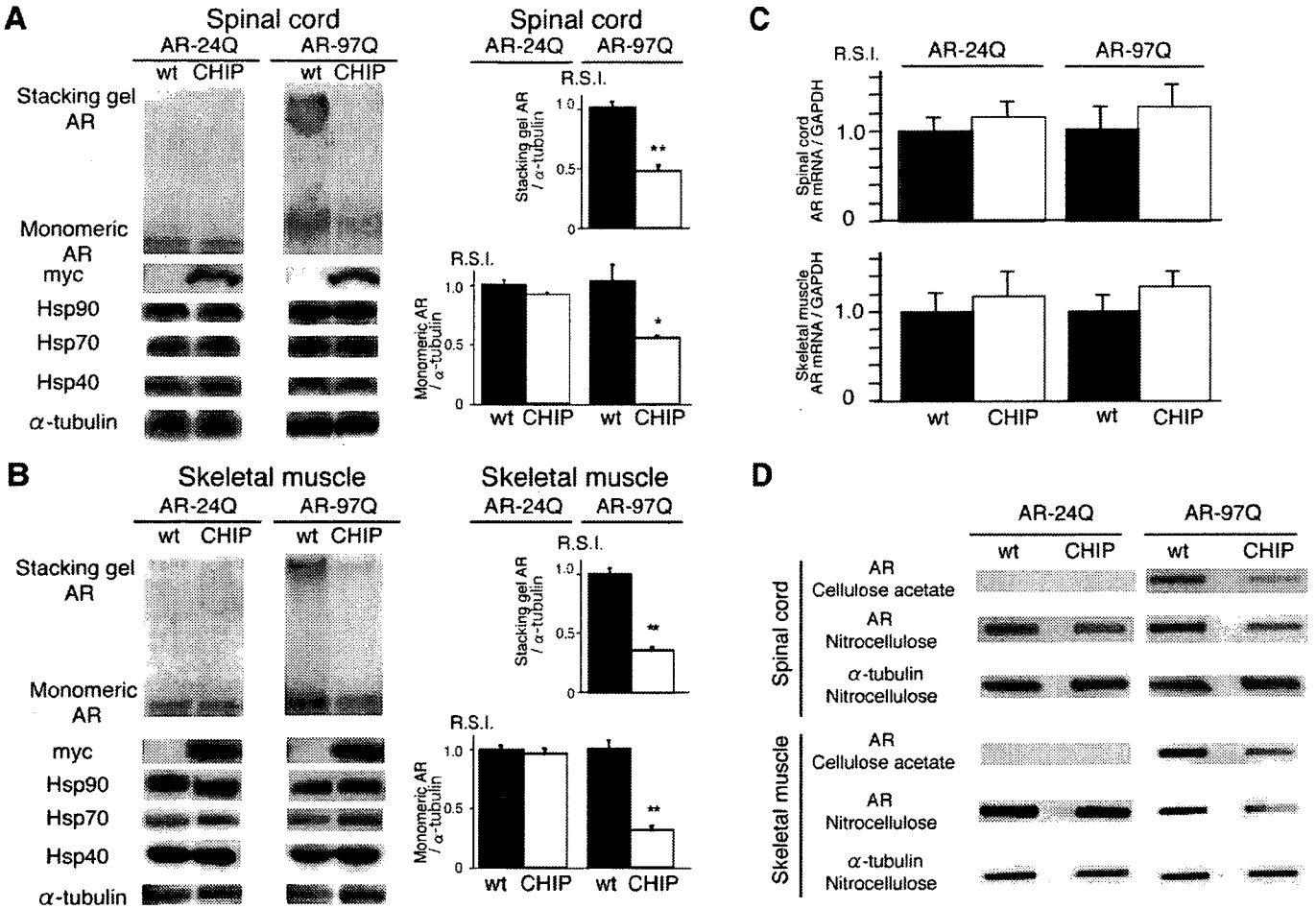

Figure 6. CHIP decreases mutant AR protein complexes as well as monomeric mutant AR. ***A***, ***B***, Western blot analysis of total tissue homogenates from the spinal cord (***A***) and muscle (***B***) of AR-24Q/CHIP$^{(-/-)}$, AR-24Q/CHIP$^{(tg/tg)}$, AR-97Q/CHIP$^{(-/-)}$, and AR-97Q/CHIP$^{(tg/tg)}$ mice (16-week-old) probed with an AR-specific antibody (H280). The mutant AR complex appears in the stacking gel, and the monomeric mutant AR appears in the separating gel. Values are expressed as mean ± SEM for six mice. $*p < 0.001$; $**p < 0.0001$. ***C***, Real-time RT-PCR of wild-type (AR-24Q) and mutant AR (AR-97Q) mRNA in transgenic mouse spinal cord and skeletal muscle in the absence (wt) and presence (CHIP) of CHIP overexpression. Values are expressed as means ± SE ($n = 6$). ***D***, Filter trap assay of total tissue homogenates from the spinal cord and muscle of AR-97Q/CHIP$^{(-/-)}$ and AR-97Q/CHIP$^{(tg/tg)}$ mice (16 weeks of age), in the absence and presence of CHIP overexpression. Homogenates were filtrated and immunolabeled with an antibody against AR (H280). Large aggregated mutant AR complexes were trapped by the cellulose acetate membrane; soluble monomeric mutant AR passed through the cellulose acetate membrane and was trapped by the nitrocellulose membrane. Endogenous α-tubulin was used as a loading control.

symptom-relief therapies, such as L-DOPA for Parkinson's disease, these disease-modifying therapies inhibit or slow down the pathogenic processes of neuronal degeneration.

CHIP interacts with Hsp90 or Hsp70, ubiquitylates unfolded proteins trapped by molecular chaperones, and degrades them, thus acting as a quality control E3 ubiquitin ligase (Murata et al., 2001). The remarkable reduction of monomeric mutant AR in the AR-97Q/CHIP mice may reflect accelerated degradation of mutant AR through the CHIP-mediated E3-proteasome system. CHIP also ubiquitinated the AR protein in a polyQ length-dependent manner, suggesting that overexpression of CHIP enhances the degradation of monomeric mutant AR by activating the Hsp70-interacting, quality control E3 system. This subsequently reduces the amount of nuclear-localized mutant AR, resulting in amelioration of phenotypic expression induced by mutant AR. Interaction between Hsp70 and CHIP, detected by coimmunoprecipitation and Western blot analysis, in the double-transgenic mice supports this view. Increased activity of CHIP was reported to modify a neurodegenerative phenotype caused by expanded ataxin-1 and huntingtin in a chaperone-dependent manner in cellular and *Drosophila* models (Jana et al., 2005; Al-Ramahi et al., 2006). CHIP lacking the normal TPR domain did not ubiquitinate the ataxin-1 protein (Al-Ramahi et al., 2006). These results suggest that chaperone interaction is essential for CHIP-dependent ubiquitination. Hsp70 overexpression in cell culture and mouse models of SBMA enhanced degradation of mutant AR-polyQ protein via its interaction with the ubiquitin-proteasome system (Bailey et al., 2002; Adachi et al., 2003). CHIP might be one such coupling factor between the Hsp70 chaperone system and the machinery responsible for degrading mutant AR. Another possibility is that overexpression of CHIP may accelerate chaperone-independent interaction with mutant AR and its degradation through the proteasome pathway. CHIP directly interacts with and degrades the AR protein (He et al., 2004; Rees et al., 2006). Thus, the interactions we demonstrated between CHIP and AR may be either direct or mediated by chaperones that are known to interact with CHIP. This direct interaction of CHIP with the AR protein might promote mutant AR degradation through the proteasome system.

Accumulation of misfolded proteins is causally related to

many age-related neurodegenerative diseases (Muchowski and Wacker, 2005; Bates, 2006). Prompt removal and/or refolding may be required more in aged or damaged cells than in young healthy cells in which appropriate protein quality control systems function (Wickner et al., 1999). In SBMA patients, diffuse nuclear accumulation of mutant AR is frequent and extensive, being distributed in a wide array of CNS nuclei and in visceral organs (Adachi et al., 2005). In this study, we demonstrated that overexpression of CHIP significantly ameliorates the phenotypes of SBMA transgenic mice, by reducing the amount of both the monomeric and large aggregated forms of nuclear-accumulated mutant AR protein, suggesting that CHIP may change the triage of mutant AR and promote its degradation by the proteasome system (Marques et al., 2006). Thus, CHIP overexpression might provide a potential therapeutic avenue for SBMA and other polyQ diseases.

References

Adachi H, Kume A, Li M, Nakagomi Y, Niwa H, Do J, Sang C, Kobayashi Y, Doyu M, Sobue G (2001) Transgenic mice with an expanded CAG repeat controlled by the human AR promoter show polyglutamine nuclear inclusions and neuronal dysfunction without neuronal cell death. Hum Mol Genet 10:1039–1048.

Adachi H, Katsuno M, Minamiyama M, Sang C, Pagoulatos G, Angelidis C, Kusakabe M, Yoshiki A, Kobayashi Y, Doyu M, Sobue G (2003) Heat shock protein 70 chaperone overexpression ameliorates phenotypes of the spinal and bulbar muscular atrophy transgenic mouse model by reducing nuclear-localized mutant androgen receptor protein. J Neurosci 23:2203–2211.

Adachi H, Katsuno M, Minamiyama M, Waza M, Sang C, Nakagomi Y, Kobayashi Y, Tanaka F, Doyu M, Inukai A, Yoshida M, Hashizume Y, Sobue G (2005) Widespread nuclear and cytoplasmic accumulation of mutant androgen receptor in SBMA patients. Brain 128:659–670.

Al-Ramahi I, Lam YC, Chen HK, de Gouyon B, Zhang M, Perez AM, Branco J, de Haro M, Patterson C, Zoghbi HY, Botas J (2006) CHIP protects from the neurotoxicity of expanded and wild-type ataxin-1 and promotes their ubiquitination and degradation. J Biol Chem 281:26714–26724.

Atsuta N, Watanabe H, Ito M, Banno H, Suzuki K, Katsuno M, Tanaka F, Tamakoshi A, Sobue G (2006) Natural history of spinal and bulbar muscular atrophy (SBMA): a study of 223 Japanese patients. Brain 129:1446–1455.

Bailey CK, Andriola IF, Kampinga HH, Merry DE (2002) Molecular chaperones enhance the degradation of expanded polyglutamine repeat androgen receptor in a cellular model of spinal and bulbar muscular atrophy. Hum Mol Genet 11:515–523.

Ballinger CA, Connell P, Wu Y, Hu Z, Thompson LJ, Yin LY, Patterson C (1999) Identification of CHIP, a novel tetratricopeptide repeat-containing protein that interacts with heat shock proteins and negatively regulates chaperone functions. Mol Cell Biol 19:4535–4545.

Banno H, Adachi H, Katsuno M, Suzuki K, Atsuta N, Watanabe H, Tanaka F, Doyu M, Sobue G (2006) Mutant androgen receptor accumulation in spinal and bulbar muscular atrophy scrotal skin: a pathogenic marker. Ann Neurol 59:520–526.

Bates GP (2006) BIOMEDICINE: One misfolded protein allows others to sneak by. Science 311:1385–1386.

Bonvini P, Dalla Rosa H, Vignes N, Rosolen A (2004) Ubiquitination and proteasomal degradation of nucleophosmin-anaplastic lymphoma kinase induced by 17-allylamino-demethoxygeldanamycin: role of the co-chaperone carboxyl heat shock protein 70-interacting protein. Cancer Res 64:3256–3264.

Cardozo CP, Michaud C, Ost MC, Fliss AE, Yang E, Patterson C, Hall SJ, Caplan AJ (2003) C-terminal Hsp-interacting protein slows androgen receptor synthesis and reduces its rate of degradation. Arch Biochem Biophys 410:134–140.

Chavez Zobel AT, Loranger A, Marceau N, Theriault JR, Lambert H, Landry J (2003) Distinct chaperone mechanisms can delay the formation of aggresomes by the myopathy-causing R120G alphaB-crystallin mutant. Hum Mol Genet 12:1609–1620.

Chevalier-Larsen ES, O'Brien CJ, Wang H, Jenkins SC, Holder L, Lieberman AP, Merry DE (2004) Castration restores function and neurofilament alterations of aged symptomatic males in a transgenic mouse model of spinal and bulbar muscular atrophy. J Neurosci 24:4778–4786.

Connell P, Ballinger CA, Jiang J, Wu Y, Thompson LJ, Hohfeld J, Patterson C (2001) The co-chaperone CHIP regulates protein triage decisions mediated by heat-shock proteins. Nat Cell Biol 3:93–96.

Cummings CJ, Mancini MA, Antalffy B, DeFranco DB, Orr HT, Zoghbi HY (1998) Chaperone suppression of aggregation and altered subcellular proteasome localization imply protein misfolding in SCA1. Nat Genet 19:148–154.

Cyr DM, Hohfeld J, Patterson C (2002) Protein quality control: U-box-containing E3 ubiquitin ligases join the fold. Trends Biochem Sci 27:368–375.

Dai Q, Zhang C, Wu Y, McDonough H, Whaley RA, Godfrey V, Li HH, Madamanchi N, Xu W, Neckers L, Cyr D, Patterson C (2003) CHIP activates HSF1 and confers protection against apoptosis and cellular stress. EMBO J 22:5446–5458.

Daviau A, Proulx R, Robitaille K, Di Fruscio M, Tanguay RM, Landry J, Patterson C, Durocher Y, Blouin R (2006) Down-regulation of the mixed-lineage dual leucine zipper-bearing kinase by heat shock protein 70 and its co-chaperone CHIP. J Biol Chem 281:31467–31477.

Demand J, Alberti S, Patterson C, Hohfeld J (2001) Cooperation of a ubiquitin domain protein and an E3 ubiquitin ligase during chaperone/proteasome coupling. Curr Biol 11:1569–1577.

Dickey CA, Yue M, Lin WL, Dickson DW, Dunmore JH, Lee WC, Zehr C, West G, Cao S, Clark AM, Caldwell GA, Caldwell KA, Eckman C, Patterson C, Hutton M, Petrucelli L (2006) Deletion of the ubiquitin ligase CHIP leads to the accumulation, but not the aggregation, of both endogenous phospho- and caspase-3-cleaved tau species. J Neurosci 26:6985–6996.

Di Prospero NA, Fischbeck KH (2005) Therapeutics development for triplet repeat expansion diseases. Nat Rev Genet 6:756–765.

Doyu M, Sobue G, Mukai E, Kachi T, Yasuda T, Mitsuma T, Takahashi A (1992) Severity of X-linked recessive bulbospinal neuronopathy correlates with size of the tandem CAG repeat in androgen receptor gene. Ann Neurol 32:707–710.

Esser C, Scheffner M, Hohfeld J (2005) The chaperone-associated ubiquitin ligase CHIP is able to target p53 for proteasomal degradation. J Biol Chem 280:27443–27448.

Gatchel JR, Zoghbi HY (2005) Diseases of unstable repeat expansion: mechanisms and common principles. Nat Rev Genet 6:743–755.

Grelle G, Kostka S, Otto A, Kersten B, Genser KF, Muller EC, Walter S, Boddrich A, Stelzl U, Hanig C, Volkmer-Engert R, Landgraf C, Alberti S, Hohfeld J, Strodicke M, Wanker EE (2006) Identification of VCP/p97, carboxyl terminus of Hsp70-interacting protein (CHIP), and amphiphysin II interaction partners using membrane-based human proteome arrays. Mol Cell Proteomics 5:234–244.

Hatakeyama S, Yada M, Matsumoto M, Ishida N, Nakayama KI (2001) U box proteins as a new family of ubiquitin-protein ligases. J Biol Chem 276:33111–33120.

Hatakeyama S, Matsumoto M, Kamura T, Murayama M, Chui DH, Planel E, Takahashi R, Nakayama KI, Takashima A (2004) U-box protein carboxyl terminus of Hsc70-interacting protein (CHIP) mediates polyubiquitylation preferentially on four-repeat Tau and is involved in neurodegeneration of tauopathy. J Neurochem 91:299–307.

He B, Bai S, Hnat AT, Kalman RI, Minges JT, Patterson C, Wilson EM (2004) An androgen receptor NH2-terminal conserved motif interacts with the COOH terminus of the Hsp70-interacting protein (CHIP). J Biol Chem 279:30643–30653.

Huang Z, Nie L, Xu M, Sun XH (2004) Notch-induced E2A degradation requires CHIP and Hsc70 as novel facilitators of ubiquitination. Mol Cell Biol 24:8951–8962.

Hwang JR, Zhang C, Patterson C (2005) C-terminus of heat shock protein 70-interacting protein facilitates degradation of apoptosis signal-regulating kinase 1 and inhibits apoptosis signal-regulating kinase 1-dependent apoptosis. Cell Stress Chaperones 10:147–156.

Igarashi S, Tanno Y, Onodera O, Yamazaki M, Sato S, Ishikawa A, Miyatani N, Nagashima M, Ishikawa Y, Sahashi K, Ibi T, Miyatake T, Tsuji S (1992) Strong correlation between the number of CAG repeats in androgen receptor genes and the clinical onset of features of spinal and bulbar muscular atrophy. Neurology 42:2300–2302.

Ishigaki S, Liang Y, Yamamoto M, Niwa J, Ando Y, Yoshihara T, Takeuchi H, Doyu M, Sobue G (2002) X-linked inhibitor of apoptosis protein is in-

volved in mutant SOD1-mediated neuronal degeneration. J Neurochem 82:576–584.

Jana NR, Dikshit P, Goswami A, Kotliarova S, Murata S, Tanaka K, Nukina N (2005) Co-chaperone CHIP associates with expanded polyglutamine protein and promotes their degradation by proteasomes. J Biol Chem 280:11635–11640.

Jiang J, Ballinger CA, Wu Y, Dai Q, Cyr DM, Hohfeld J, Patterson C (2001) CHIP is a U-box-dependent E3 ubiquitin ligase: identification of Hsc70 as a target for ubiquitylation. J Biol Chem 276:42938–42944.

Katsuno M, Adachi H, Kume A, Li M, Nakagomi Y, Niwa H, Sang C, Kobayashi Y, Doyu M, Sobue G (2002) Testosterone reduction prevents phenotypic expression in a transgenic mouse model of spinal and bulbar muscular atrophy. Neuron 35:843–854.

Katsuno M, Adachi H, Doyu M, Minamiyama M, Sang C, Kobayashi Y, Inukai A, Sobue G (2003) Leuprorelin rescues polyglutamine-dependent phenotypes in a transgenic mouse model of spinal and bulbar muscular atrophy. Nat Med 9:768–773.

Katsuno M, Sang C, Adachi H, Minamiyama M, Waza M, Tanaka F, Doyu M, Sobue G (2005) Pharmacological induction of heat-shock proteins alleviates polyglutamine-mediated motor neuron disease. Proc Natl Acad Sci USA 102:16801–16806.

Katsuno M, Adachi H, Minamiyama M, Waza M, Tokui K, Banno H, Suzuki K, Onoda Y, Tanaka F, Doyu M, Sobue G (2006) Reversible disruption of dynactin 1-mediated retrograde axonal transport in polyglutamine-induced motor neuron degeneration. J Neurosci 26:12106–12117.

Kennedy WR, Alter M, Sung JH (1968) Progressive proximal spinal and bulbar muscular atrophy of late onset. A sex-linked recessive trait. Neurology 18:671–680.

Kobayashi Y, Kume A, Li M, Doyu M, Hata M, Ohtsuka K, Sobue G (2000) Chaperones Hsp70 and Hsp40 suppress aggregate formation and apoptosis in cultured neuronal cells expressing truncated androgen receptor protein with expanded polyglutamine tract. J Biol Chem 275:8772–8778.

La Spada AR, Wilson EM, Lubahn DB, Harding AE, Fischbeck KH (1991) Androgen receptor gene mutations in X-linked spinal and bulbar muscular atrophy. Nature 352:77–79.

La Spada AR, Roling DB, Harding AE, Warner CL, Spiegel R, Hausmanowa-Petrusewicz I, Yee WC, Fischbeck KH (1992) Meiotic stability and genotype-phenotype correlation of the trinucleotide repeat in X-linked spinal and bulbar muscular atrophy. Nat Genet 2:301–304.

Li M, Miwa S, Kobayashi Y, Merry DE, Yamamoto M, Tanaka F, Doyu M, Hashizume Y, Fischbeck KH, Sobue G (1998a) Nuclear inclusions of the androgen receptor protein in spinal and bulbar muscular atrophy. Ann Neurol 44:249–254.

Li M, Nakagomi Y, Kobayashi Y, Merry DE, Tanaka F, Doyu M, Mitsuma T, Hashizume Y, Fischbeck KH, Sobue G (1998b) Nonneural nuclear inclusions of androgen receptor protein in spinal and bulbar muscular atrophy. Am J Pathol 153:695–701.

Lieberman AP, Harmison G, Strand AD, Olson JM, Fischbeck KH (2002) Altered transcriptional regulation in cells expressing the expanded polyglutamine androgen receptor. Hum Mol Genet 11:1967–1976.

Marques C, Guo W, Pereira P, Taylor A, Patterson C, Evans PC, Shang F (2006) The triage of damaged proteins: degradation by the ubiquitin-proteasome pathway or repair by molecular chaperones. FASEB J 20:741–743.

McClellan AJ, Tam S, Kaganovich D, Frydman J (2005) Protein quality control: chaperones culling corrupt conformations. Nat Cell Biol 7:736–741.

McDonough H, Patterson C (2003) CHIP: a link between the chaperone and proteasome systems. Cell Stress Chaperones 8:303–308.

Meacham GC, Patterson C, Zhang W, Younger JM, Cyr DM (2001) The Hsc70 co-chaperone CHIP targets immature CFTR for proteasomal degradation. Nat Cell Biol 3:100–105.

Miller VM, Nelson RF, Gouvion CM, Williams A, Rodriguez-Lebron E, Harper SQ, Davidson BL, Rebagliati MR, Paulson HL (2005) CHIP suppresses polyglutamine aggregation and toxicity *in vitro* and *in vivo*. J Neurosci 25:9152–9161.

Minamiyama M, Katsuno M, Adachi H, Waza M, Sang C, Kobayashi Y, Tanaka F, Doyu M, Inukai A, Sobue G (2004) Sodium butyrate ameliorates phenotypic expression in a transgenic mouse model of spinal and bulbar muscular atrophy. Hum Mol Genet 13:1183–1192.

Muchowski PJ, Wacker JL (2005) Modulation of neurodegeneration by molecular chaperones. Nat Rev Neurosci 6:11–22.

Murata S, Minami Y, Minami M, Chiba T, Tanaka K (2001) CHIP is a chaperone-dependent E3 ligase that ubiquitylates unfolded protein. EMBO Rep 2:1133–1138.

Murata S, Chiba T, Tanaka K (2003) CHIP: a quality-control E3 ligase collaborating with molecular chaperones. Int J Biochem Cell Biol 35:572–578.

Niwa H, Yamamura K, Miyazaki J (1991) Efficient selection for high-expression transfectants with a novel eukaryotic vector. Gene 108:193–199.

Petrucelli L, Dickson D, Kehoe K, Taylor J, Snyder H, Grover A, De Lucia M, McGowan E, Lewis J, Prihar G, Kim J, Dillmann WH, Browne SE, Hall A, Voellmy R, Tsuboi Y, Dawson TM, Wolozin B, Hardy J, Hutton M (2004) CHIP and Hsp70 regulate tau ubiquitination, degradation and aggregation. Hum Mol Genet 13:703–714.

Poletti A, Negri-Cesi P, Martini L (2005) Reflections on the diseases linked to mutations of the androgen receptor. Endocrine 28:243–262.

Qian SB, McDonough H, Boellmann F, Cyr DM, Patterson C (2006) CHIP-mediated stress recovery by sequential ubiquitination of substrates and Hsp70. Nature 440:551–555.

Rees I, Lee S, Kim H, Tsai FT (2006) The E3 ubiquitin ligase CHIP binds the androgen receptor in a phosphorylation-dependent manner. Biochim Biophys Acta 1764:1073–1079.

Ross CA, Pickart CM (2004) The ubiquitin-proteasome pathway in Parkinson's disease and other neurodegenerative diseases. Trends Cell Biol 14:703–711.

Ross CA, Poirier MA (2004) Protein aggregation and neurodegenerative disease. Nat Med 10 [Suppl]:S10–S17.

Sahara N, Murayama M, Mizoroki T, Urushitani M, Imai Y, Takahashi R, Murata S, Tanaka K, Takashima A (2005) In vivo evidence of CHIP up-regulation attenuating tau aggregation. J Neurochem 94:1254–1263.

Schmidt T, Lindenberg KS, Krebs A, Schols L, Laccone F, Herms J, Rechsteiner M, Riess O, Landwehrmeyer GB (2002) Protein surveillance machinery in brains with spinocerebellar ataxia type 3: redistribution and differential recruitment of 26S proteasome subunits and chaperones to neuronal intranuclear inclusions. Ann Neurol 51:302–310.

Shin Y, Klucken J, Patterson C, Hyman BT, McLean PJ (2005) The co-chaperone carboxyl terminus of Hsp70-interacting protein (CHIP) mediates alpha-synuclein degradation decisions between proteasomal and lysosomal pathways. J Biol Chem 280:23727–23734.

Slow EJ, Graham RK, Hayden MR (2006) To be or not to be toxic: aggregations in Huntington and Alzheimer disease. Trends Genet 22:408–411.

Sobue G, Hashizume Y, Mukai E, Hirayama M, Mitsuma T, Takahashi A (1989) X-linked recessive bulbospinal neuronopathy. A clinicopathological study. Brain 112:209–232.

Sobue G, Doyu M, Kachi T, Yasuda T, Mukai E, Kumagai T, Mitsuma T (1993) Subclinical phenotypic expressions in heterozygous females of X-linked recessive bulbospinal neuronopathy. J Neurol Sci 117:74–78.

Sopher BL, Thomas Jr PS., LaFevre-Bernt MA, Holm IE, Wilke SA, Ware CB, Jin LW, Libby RT, Ellerby LM, La Spada AR (2004) Androgen receptor YAC transgenic mice recapitulate SBMA motor neuronopathy and implicate VEGF164 in the motor neuron degeneration. Neuron 41:687–699.

Sperfeld AD, Karitzky J, Brummer D, Schreiber H, Haussler J, Ludolph AC, Hanemann CO (2002) X-linked bulbospinal neuronopathy: Kennedy disease. Arch Neurol 59:1921–1926.

Stenoien DL, Cummings CJ, Adams HP, Mancini MG, Patel K, DeMartino GN, Marcelli M, Weigel NL, Mancini MA (1999) Polyglutamine-expanded androgen receptors form aggregates that sequester heat shock proteins, proteasome components and SRC-1, and are suppressed by the HDJ-2 chaperone. Hum Mol Genet 8:731–741.

Tanaka F, Doyu M, Ito Y, Matsumoto M, Mitsuma T, Abe K, Aoki M, Itoyama Y, Fischbeck KH, Sobue G (1996) Founder effect in spinal and bulbar muscular atrophy (SBMA). Hum Mol Genet 5:1253–1257.

Tateishi Y, Kawabe Y, Chiba T, Murata S, Ichikawa K, Murayama A, Tanaka K, Baba T, Kato S, Yanagisawa J (2004) Ligand-dependent switching of ubiquitin-proteasome pathways for estrogen receptor. EMBO J 23:4813–4823.

Thomas M, Dadgar N, Aphale A, Harrell JM, Kunkel R, Pratt WB, Lieberman AP (2004) Androgen receptor acetylation site mutations cause traffick-

ing defects, misfolding, and aggregation similar to expanded glutamine tracts. J Biol Chem 279:8389–8395.

Wang X, DeFranco DB (2005) Alternative effects of the ubiquitin-proteasome pathway on glucocorticoid receptor down-regulation and transactivation are mediated by CHIP, an E3 ligase. Mol Endocrinol 19:1474–1482.

Wanker EE, Scherzinger E, Heiser V, Sittler A, Eickhoff H, Lehrach H (1999) Membrane filter assay for detection of amyloid-like polyglutamine-containing protein aggregates. Methods Enzymol 309:375–386.

Waza M, Adachi H, Katsuno M, Minamiyama M, Sang C, Tanaka F, Inukai A, Doyu M, Sobue G (2005) 17-AAG, an Hsp90 inhibitor, ameliorates polyglutamine-mediated motor neuron degeneration. Nat Med 11:1088–1095.

Wickner S, Maurizi MR, Gottesman S (1999) Posttranslational quality control: folding, refolding, and degrading proteins. Science 286:1888–1893.

Younger JM, Chen L, Ren HY, Rosser MF, Turnbull EL, Fan CY, Patterson C, Cyr DM (2006) Sequential quality-control checkpoints triage misfolded cystic fibrosis transmembrane conductance regulator. Cell 126:571–582.

Yu Z, Dadgar N, Albertelli M, Gruis K, Jordan C, Robins DM, Lieberman AP (2006) Androgen-dependent pathology demonstrates myopathic contribution to the Kennedy disease phenotype in a mouse knock-in model. J Clin Invest 116:2663–2672.

Zhou P, Fernandes N, Dodge IL, Reddi AL, Rao N, Safran H, DiPetrillo TA, Wazer DE, Band V, Band H (2003) ErbB2 degradation mediated by the co-chaperone protein CHIP. J Biol Chem 278:13829–13837.

THE JOURNAL OF BIOLOGICAL CHEMISTRY VOL. 282, NO. 38, pp. 28087–28095, September 21, 2007

Disulfide Bond Mediates Aggregation, Toxicity, and Ubiquitylation of Familial Amyotrophic Lateral Sclerosis-linked Mutant SOD1*[S]

Received for publication, May 31, 2007, and in revised form, July 13, 2007 Published, JBC Papers in Press, July 31, 2007, DOI 10.1074/jbc.M704465200

Jun-ichi Niwa[‡§], Shin-ichi Yamada[‡], Shinsuke Ishigaki[‡], Jun Sone[‡], Miho Takahashi[‡], Masahisa Katsuno[‡], Fumiaki Tanaka[‡], Manabu Doyu[‡§], and Gen Sobue[‡1]

From the [‡]Department of Neurology, Nagoya University Graduate School of Medicine, 65 Tsurumai-cho, Showa-ku, Nagoya 466-8500 and the [§]Stroke Center, Aichi Medical University, Aichi 480-1195, Japan

Mutations in the Cu/Zn-superoxide dismutase (*SOD1*) gene cause familial amyotrophic lateral sclerosis (ALS) through the gain of a toxic function; however, the nature of this toxic function remains largely unknown. Ubiquitylated aggregates of mutant SOD1 proteins in affected brain lesions are pathological hallmarks of the disease and are suggested to be involved in several proposed mechanisms of motor neuron death. Recent studies suggest that mutant SOD1 readily forms an incorrect disulfide bond upon mild oxidative stress *in vitro*, and the insoluble SOD1 aggregates in spinal cord of ALS model mice contain multimers cross-linked via intermolecular disulfide bonds. Here we show that a non-physiological intermolecular disulfide bond between cysteines at positions 6 and 111 of mutant SOD1 is important for high molecular weight aggregate formation, ubiquitylation, and neurotoxicity, all of which were dramatically reduced when the pertinent cysteines were replaced in mutant SOD1 expressed in Neuro-2a cells. Dorfin is a ubiquityl ligase that specifically binds familial ALS-linked mutant SOD1 and ubiquitylates it, thereby promoting its degradation. We found that Dorfin ubiquitylated mutant SOD1 by recognizing the Cys^{6}- and Cys^{111}-disulfide cross-linked form and targeted it for proteasomal degradation.

Cu/Zn superoxide dismutase (SOD1),[2] a major intracellular antioxidant enzyme, metabolizes superoxide radicals to molecular oxygen and hydrogen peroxide (1, 2). Because mutations in *SOD1* linked to familial amyotrophic lateral sclerosis (ALS) were first identified (3), more than 100 mutations at over 70 residues in the 153-amino acid SOD1 protein have been reported (4). Most mutations are missense mutations, with a few causing early termination or frame shifts near the carboxyl terminus of the protein. *SOD1* mutations account for ~20% of familial ALS, which is characterized by selective degeneration of motor neurons. SOD1 is primarily a cytosolic protein (5), and the active enzyme is a homodimer of two subunits (6). Each subunit contains four cysteine (Cys) residues at positions 6, 57, 111, and 146. An intramolecular disulfide bond between Cys^{57} and Cys^{146} of each subunit facilitates its correct folding and stabilizes the active homodimeric structure (7, 8), but it is not known how the disulfide is formed in the reducing environment of the cytosol. Although the endoplasmic reticulum is the specialized site for oxidative folding (9), there is no SOD1 localization to the endoplasmic reticulum (10). Most familial ALS-linked mutations render SOD1 more susceptible to intramolecular disulfide bond reduction (11) and accelerate the rate of protein turnover (12, 13). Recent lines of evidence implicate the disulfide-reduced monomer as the common aggregation-prone, neurotoxic intermediate of mutant SOD1 proteins (8, 11, 14–16), and a significant fraction of the insoluble SOD1 aggregates in the spinal cord of mutant SOD1 transgenic mice contains high molecular weight species cross-linked via intermolecular disulfide bonds (17). Hence, modulation of disulfide bond formation may be important in mutant SOD1-linked motor neuron-selective neurotoxicity.

ALS-linked mutant SOD1 proteins are turned over more rapidly than wild-type SOD1, and proteasome inhibitors increase the amount of mutant SOD1 (18, 19). To date, two distinct ubiquityl ligases, Dorfin and NEDL1, have been reported to ubiquitylate mutant SOD1 (20, 21). Dorfin is a RING-finger/IBR (in-between ring-finger) domain-containing ubiquityl ligase, which we previously identified from human spinal cord (22), and belongs to the RBR (RING-Between rings-RING) family of proteins (23). Dorfin physically binds and ubiquitylates various familial ALS-linked SOD1 mutants and subsequently targets them for proteasomal degradation, but it has no effect on the stability of wild-type SOD1 (20). Overexpression of Dorfin protects neuronal cells against the toxic effects of mutant SOD1 and reduces the number of aggregates composed of mutant SOD1 (20). However, the mechanism by which Dorfin discriminates between the normal and pathogenic status of SOD1 proteins remains unknown. There are numerous variants causing familial ALS, thus it seems reasonable that Dorfin recognizes a common protein modification among mutant SOD1s that is not present in wild-type SOD1.

* This work was supported by a Center of Excellence grant from the Ministry of Education, Culture, Sports, Science and Technology and grants from the Ministry of Health, Labor and Welfare of Japan. The costs of publication of this article were defrayed in part by the payment of page charges. This article must therefore be hereby marked "*advertisement*" in accordance with 18 U.S.C. Section 1734 solely to indicate this fact.

[S] The on-line version of this article (available at http://www.jbc.org) contains supplemental Fig. S1.

[1] To whom correspondence should be addressed. Tel.: 81-52-744-2385; Fax: 81-52-744-2384; E-mail: sobueg@med.nagoya-u.ac.jp.

[2] The abbreviations used are: SOD1, superoxide dismutase 1; ALS, amyotrophic lateral sclerosis; 2-ME, 2-mercaptoethanol; WST-1, 4-[3-(4-iodophenyl)-2-(4-nitrophenyl)-2H-5-tetrazolio]-1,3-benzene disulfonate; GFP, green fluorescent protein.

In this study, we generated SOD1 proteins with various combinations of the four Cys residues replaced by serines and assessed their disulfide bond status, the changes in the formations of their high molecular weight species, and their neurotoxicity. Moreover, by studying the interaction between Dorfin and these engineered SOD1s, we investigated whether disulfide bonds are critical for Dorfin recognition and ubiquitylation of mutant SOD1s.

EXPERIMENTAL PROCEDURES

Construction of Expression Vectors—Construction of pcDNA3.1/MycHis-SOD1, pEGFP-N1-SOD1, and pcDNA4/HisMax-Dorfin vectors were described previously (20, 22). Cys to Ser missense mutations were introduced into pcDNA3.1/MycHis-SOD1 and pEGFP-N1-SOD1 with a QuikChange site-directed mutagenesis kit (Stratagene, La Jolla, CA). Primer pairs for each Cys to Ser mutant were as follows: 5′-CGAAGGCCGTGTCCGTGCTGAAGGGC-3′ and 5′-GCCCTTCAGCACGGACACGGCCTTCG-3′ for C6S; 5′-GATAATACAGCAGGCTCTACCAGTGCAGGTCC-3′ and 5′-GGACCTGCACTGGTAGAGCCTGCTGTATTATC-3′ for C57S; 5′-CTCAGGAGACCATTCCATCATTGGCCGCAC-3′ and 5′-GTGCGGCCAATGATGGAATGGTCTCCTGAG-3′ for C111S; and 5′-GGAAGTCGTTTGGCTTCTGGTGTAATTGGGATCG-3′ and 5′-CGATCCCAATTACACCAGAAGCCAAACGACTTCC-3 for C146S. Multiple Cys to Ser replaced vectors were obtained by repeatedly applying a mutagenesis.

Cell Culture, Transfection, and Antibodies—Neuro-2a cells (American Type Culture Collection, Manassas, VA), a line derived from mouse neuroblastoma, were maintained in Dulbecco's modified Eagle's medium containing 10% fetal calf serum, 5 units/ml penicillin, and 50 μg/ml streptomycin. Transfections were performed using Lipofectamine 2000 (Invitrogen) in the WST-1 assay or Effectene Transfection Reagent (Qiagen, Valencia, CA) in other experiments according to the manufacturers' instructions. To inhibit cellular proteasome activity, cells were treated with 1 μM (except as otherwise indicated) MG132 (Z-Leu-Leu-Leu-al, Sigma) or epoxomicin (Sigma) as indicated concentration for 24 h after overnight transfection. To differentiate Neuro-2a cells, they were changed to Dulbecco's modified Eagle's medium culture medium containing 2% fetal calf serum and 20 μM retinoic acid and cultured for 48 h. Primary antibodies used were as follows: anti-Myc mouse monoclonal antibody (9E10, Sigma), anti-Myc rabbit polyclonal antibody (A-14, Santa Cruz Biotechnology, Santa Cruz, CA), anti-SOD1 rabbit polyclonal antibody (SOD100, Stressgen Bioreagents, Victoria, Canada), anti-α-tubulin mouse monoclonal antibody (B-5-1-1, Sigma), anti-ubiquitin mouse monoclonal antibody (4PD1, Santa Cruz Biotechnology), and anti-Xpress mouse monoclonal antibody (Invitrogen).

Transgenic Mice—17-week-old symptomatic B6SJL-TgN(SOD1-G93A)1Gur ALS mice overexpressing the human mutant $SOD1^{G93A}$ (The Jackson Laboratory, Bar Harbor, ME) were used. The experimental design of this study was fully approved by the Experimental Animal Ethical Committee of the Nagoya University Graduate School of Medicine. Tissues were homogenized in 10 volumes of lysis buffer (TNE) consisting of 50 mM Tris-HCl, 150 mM NaCl, 1% Nonidet P-40, and 1 mM EDTA with a protease inhibitor mixture (Complete Mini, Roche Diagnostics, Indianapolis, IN) and centrifuged at 20,000 × *g* for 30 min at 4 °C. Supernatants were used for Western blotting analysis.

Immunoprecipitation and Western Blotting Analysis—5×10^5 cells from a 6-cm dish were lysed on ice with 1 ml of TNE lysis buffer. The lysate was centrifuged at 1,000 × *g* for 15 min at 4 °C to remove nuclei and cell debris. Denucleated cell lysates (crude fraction) were separated into supernatant (soluble fraction) and pellet fractions by centrifuging at 20,000 × *g* for 20 min at 4 °C. The pellets were lysed (insoluble fraction) with 1 ml of TNES lysis buffer consisting of 50 mM Tris-HCl, 150 mM NaCl, 1% Nonidet P-40, 2% SDS, and 1 mM EDTA with a protease inhibitor mixture (Complete Mini, Roche Diagnostics). Protein concentrations were determined with a DC protein assay kit (Bio-Rad). Immunoprecipitation from the soluble fraction was performed with 2 μg of anti-Myc or anti-Xpress antibodies and Protein A/G Plus-agarose (Santa Cruz Biotechnology), and the precipitates were washed four times in TNE buffer. Cell lysates or immunoprecipitates were separated by SDS-PAGE (5–20% gradient gel) and analyzed by Western blotting with ECL plus detection reagents (GE Healthcare Bio-Sciences, Piscataway, NJ). Non-reducing SDS-PAGE was conducted without 2-mercaptoethanol (2-ME) in the sample buffer. Because omitting reducing agents from the protein samples can lead to adventitious air oxidation or disulfide scrambling, 100 mM iodoacetamide was added to the lysates to prevent these changes during sample preparation.

Filter Trap Assay—Each of the various fractions from the cell lysates (crude, soluble, and insoluble fractions) was filtered under vacuum through 0.2-μm cellulose acetate membranes (Sartorius, Gottingen, Germany) followed by two washes in Tris-buffered saline. The membranes were then incubated with 5% milk powder in Tris-buffered saline at room temperature for 1 h, followed by an overnight incubation at 4 °C with anti-Myc antibody in Tris-buffered saline with 0.1% Tween 20. Primary antibodies were detected with horseradish peroxidase-conjugated secondary antibodies (GE Healthcare Bio-Sciences), which were then detected with ECL plus chemiluminescence reagent (GE Healthcare Bio-Sciences). To confirm equal loading of proteins, the same samples were blotted onto 0.45-μm nitrocellulose membranes (Bio-Rad) and probed with anti-Myc or anti-α-tubulin antibodies.

Neurotoxicity Analysis and Quantification of SOD1 Aggregates—2×10^4 Neuro-2a cells were grown overnight on four-chamber, collagen-coated slides (Nalge Nunc, Rochester, NY) and then transfected with 0.2 μg of pEGFP-N1-SOD1. After overnight incubation, the cells were differentiated in Dulbecco's modified Eagle's medium containing 2% fetal calf serum and 20 μM retinoic acid for 48 h. Inclusion bodies were counted in more than 100 randomly selected cells, and the percentages of cells with such inclusions were calculated. Data from three independent experiments were averaged. For the cell viability assay, 5×10^3 Neuro-2a cells were grown in 96-well collagen-coated plates overnight, and then transfected with 0.1 μg of pEGFP-N1-SOD1 or pcDNA3.1/MycHis-SOD1, with or without 0.1 μg of pcDNA4/HisMax-Dorfin. pcDNA4/HisMax

mock vector was used as a control. A 4-[3-(4-iodophenyl)-2-(4-nitrophenyl)-2H-5-tetrazolio]-1,3-benzene disulfonate (WST-1)-based cell proliferation assay (Roche Diagnostics) was performed 48 h after differentiation. Absorbance was measured in a multiple plate reader (PowerscanHT, Dainippon Pharmaceutical, Japan). The assay was carried out in triplicate and statistically analyzed by one-way analysis of variance or unpaired *t* test.

Quantitative Analysis of Gene Expression Levels—Total RNA was extracted from Neuro-2a cells expressing SOD1-GFP and their Cys to Ser derivatives by using an RNA Easy Kit (Qiagen), followed by cDNA synthesis primed with oligo(dT) using Superscript II (Invitrogen). The gene expression level was examined by quantitative reverse transcription-PCR using primer sets specific to target genes and QuantiTect SYBR Green PCR kit (Qiagen). PCR was performed on an iCycler system (Bio-Rad) under the manufacturer's recommended conditions.

Isolation of SOD1 Aggregates—Isolation of SOD1 inclusion bodies was carried out according to Lee *et al.* (24) with a slight modification. 5×10^5 Neuro-2a cells in a 60-mm dish expressing SOD1-GFP were washed with cold phosphate-buffered saline before addition of TNE buffer. After a 5-min incubation at room temperature, the supernatant containing Nonidet P-40-soluble proteins was carefully removed from dishes. After gentle washing of dishes with phosphate-buffered saline, the Nonidet P-40-insoluble materials were scraped and incubated on ice for 5 min. The extract was then centrifuged at $80 \times g$ for 15 min. The pellet containing big inclusions was put onto a slide glass, sealed with a coverslip, and observed under a BX51 epifluorescence microscope (Olympus, Tokyo, Japan).

Cycloheximide Chase Analysis—Neuro-2a cells grown on 6-cm dishes were transfected with 1 μg of pcDNA3.1/MycHis-SOD1 with or without 1 μg of pcDNA4/HisMax-Dorfin. 24 h after transfection, cycloheximide (50 μg/ml) was added to the culture medium, and the cells were harvested at the indicated time points. The samples were subjected to SDS-PAGE and analyzed by Western blotting with anti-Myc antibody. The intensities of the bands were quantified by ImageGauge software (Fuji Film, Tokyo, Japan). The assay was carried out in triplicate and statistically analyzed by one-way analysis of variance or unpaired *t* test.

RESULTS

Proteasome Inhibition Increases SDS-resistant Disulfide-linked Species as Well as Insoluble Ones of ALS-linked Mutant SOD1—Mutant SOD1 is a fairly unstable protein, and the increased turnover of mutant SOD1 is mediated by the ubiquitin-proteasome pathway (18, 19). Thus, we first examined the effect of proteasome inhibition on mutant SOD1 proteins. When cellular proteasome activity was blocked by the proteasome inhibitor MG132, the level of soluble mutant $SOD1^{G85R}$ and $SOD1^{G93A}$ increased in a dose-dependent manner (Fig. 1*B*, *arrowhead*), and an SDS-resistant mutant SOD1 dimer appeared (Fig. 1*B*, *arrow*). The increase in the amount of wild-type SOD1 was much smaller than that of mutant SOD1 (Fig. 1*B*, *arrowhead*). Detergent-insoluble, sedimentable mutant SOD1 also increased as proteasome activity was inhibited (Fig. 1*C*). Interestingly, as the proteasome activity was inhibited, aberrant high molecular weight SDS-resistant disulfide-linked mutant $SOD1^{G85R}$ and $SOD1^{G93A}$ became more abundant (Fig. 1*A*, *asterisk*). There were almost no SDS-resistant disulfide-linked species of the wild-type SOD1. The same findings were obtained when blots were probed with anti-SOD1 antibody (supplemental Fig. S1*A*). These results were also confirmed with epoxomicin, a selective and irreversible proteasome inhibitor (supplemental Fig. S1*B*). Thus, intermolecular disulfide bond-linked mutant SOD1 is unstable and prone to degradation by the proteasome.

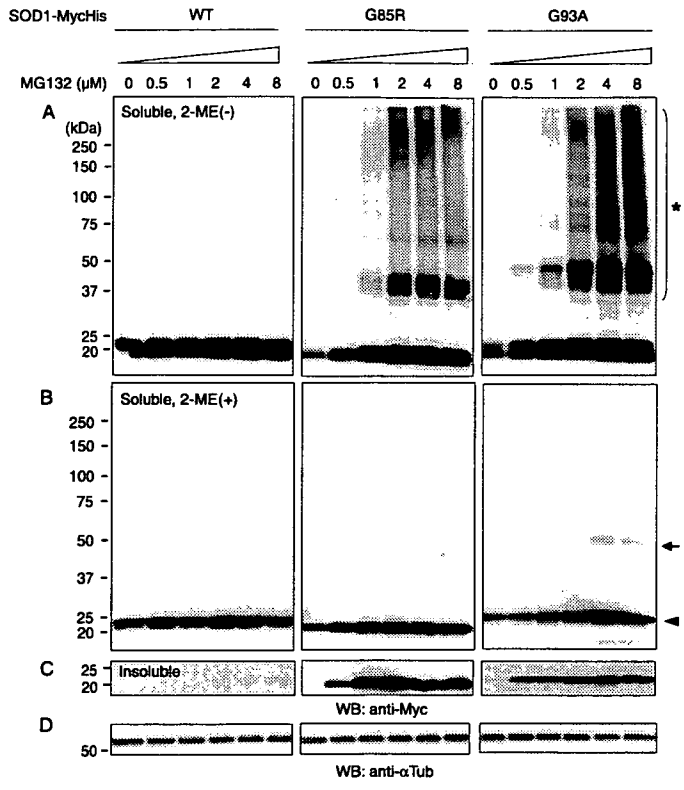

FIGURE 1. **Proteasome inhibition leads to the accumulation of intermolecular disulfide bond-linked mutant SOD1.** Neuro-2a cells expressing wild-type (*WT*), G85R, and G93A mutant SOD1-MycHis were treated with MG132 for 24 h at the indicated concentrations. Soluble fractions were analyzed by SDS-PAGE in the absence (*A*) or presence (*B*) of 2-ME. Insoluble fractions were analyzed by SDS-PAGE in the presence of 2-ME (*C*). *Arrow*, a soluble SDS-resistant dimer; *arrowhead*, a soluble monomeric SOD1; *asterisk*, disulfide-linked high molecular weight-species of SOD1. *D*, anti-α-tubulin as loading control.

Free Cys^6 and Cys^{111} Are Important for Generating Disulfide Bond-linked Species and Insoluble, Sedimentable Forms of Mutant Human SOD1—We examined the role of Cys residues in the formation of aberrant disulfide-bond linked high molecular weight species. Various combinations of the four Cys residues at positions 6, 57, 111, and 146 replaced with serines were introduced into SOD1 protein-expression vectors using site-directed mutagenesis. The effects of amino acid replacement at one of the four Cys residues, at two of the four Cys residues, and at all four Cys residues on wild-type and two familial ALS-linked SOD1 mutants, $SOD1^{G85R}$ and $SOD1^{G93A}$, were investigated. We used Myc-His-tagged SOD1 expression vectors and an antibody against the tag peptide to detect SOD1 protein so as to avoid possible reduced detection of SOD1 with multiple

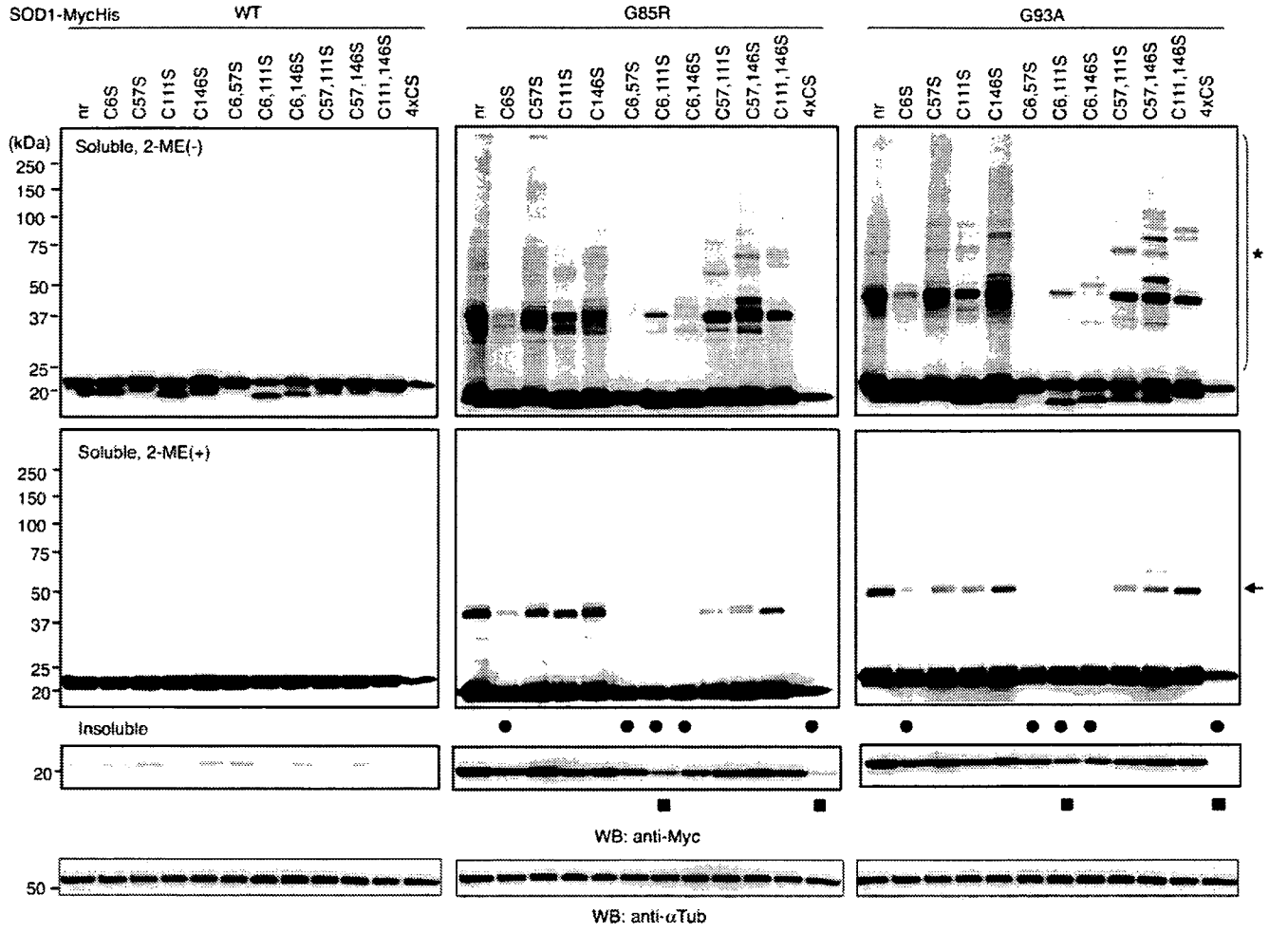

FIGURE 2. **Free Cys^6 and Cys^{111} are important for generating intermolecular disulfide-linked species and insoluble, sedimentable forms of mutant human SOD1.** Various combinations of replacing Cys with Ser were introduced into wild-type (*WT*) and mutant (G85R and G93A) SOD1-MycHis. Neuro-2a cells expressing SOD1-MycHis were treated with 2 μM MG132 for 24 h. Soluble fractions were analyzed by SDS-PAGE in the absence (*upper panels*) or presence (*middle panels*) of 2-ME. Insoluble fractions were analyzed by SDS-PAGE in the presence of 2-ME (*lower panels*). *Asterisk*, a disulfide-linked high molecular weight species; *arrow*, an SDS-resistant dimer of mutant SOD1. *Filled circles*, marked reduction of an SDS-resistant dimer with a Cys^6 replacement of mutant SOD1; *filled squares*, further reduction of the detergent-insoluble, sedimentable form of mutant SOD1 with simultaneous Cys^6 and Cys^{111} replacements. *nr*, SOD1 without replacement in cysteine residue; *4×CS*, all four cysteines replaced by serines.

amino acids changes by the anti-SOD1 antibody. Interestingly, none of the Cys residue replacements generated disulfide-linked species in wild-type SOD1 proteins (Fig. 2, *left panel*). Under reducing conditions, replacement of Cys^6 had a stronger effect on the formation of disulfide-linked species of mutant SOD1 than did the other three Cys residue replacements (Fig. 2, *middle* and *right panels*, *asterisk*). Combinations of replacing Cys^6 and one of the other Cys residues further attenuated the aberrant disulfide-linking of mutant SOD1 seen with the single substitution of Cys^6 (Fig. 2, *filled circle*). Under usual reducing conditions, the same reduced oligomerization of mutant SOD1 was observed when combinations of Cys^6 and other Cys residues were replaced (Fig. 2, *arrow*). The detergent-insoluble, sedimentable form of mutant SOD1 was also reduced especially if both Cys^6 and Cys^{111} were replaced (Fig. 2, *filled square*). Replacement of all four Cys residues completely abolished the disulfide-linked species in the non-reducing condition and the oligomeric, detergent-insoluble form of mutant SOD1 in the reducing condition (Fig. 2, *lane 4×CS*). Because simultaneous substitutions of Cys^6 and Cys^{111} had the strongest effects on the formation of aberrant species of mutant SOD1 in both non-reducing and reducing conditions, we compared C6S and C111S mutants with C57S and C146S mutants in the following experiments.

Substituting Both Cys^6 and Cys^{111} Greatly Reduces High Molecular Weight Aggregate Formation and Ubiquitylation of Mutant SOD1—In studies of polyglutamine disorders, it has been demonstrated that high molecular weight aggregates of mutant proteins are retained by filtration through cellulose acetate (25, 26). Cellulose acetate membranes usually bind protein very poorly and are used to trap high molecular weight structures from complex mixtures through filtration. This assay was also successfully applied to detect mutant SOD1 aggregation (27). Thus we used a cellulose acetate filter trap assay to investigate whether SOD1 proteins with Cys substitutions are retained in high molecular weight aggregates from lysates of SOD1-MycHis expressing Neuro-2a cells. Cells were lysed in TNE buffer, fractionated into crude denucleated, soluble, and insoluble fractions, and each fraction was then filtered through a 0.22-μm cellulose acetate membrane. Subsequent staining

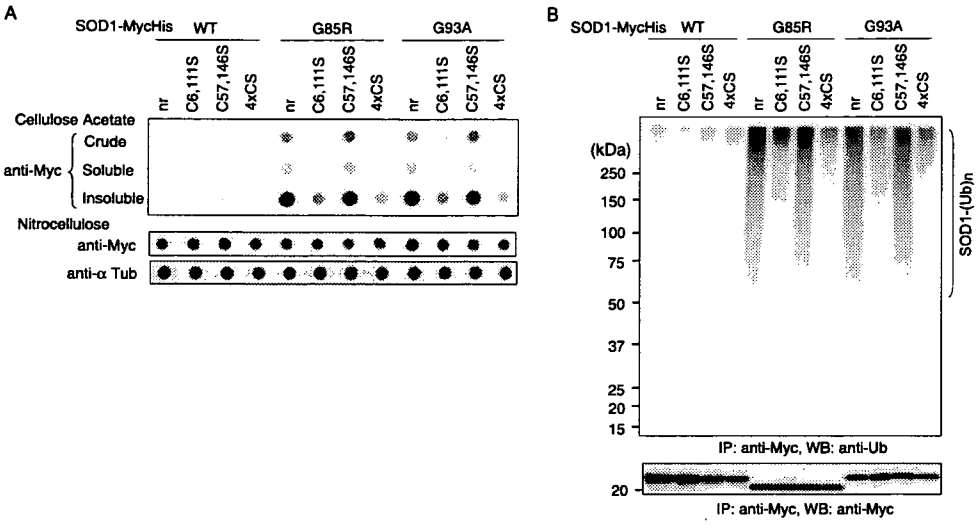

FIGURE 3. **Replacing both Cys^6 and Cys^{111} greatly reduces high molecular weight aggregate formation and ubiquitylation of mutant SOD1-MycHis.** *A*, crude, soluble, and insoluble fractions of cell lysates were analyzed by filter trap assay (*upper panel*). Nitrocellulose dot blots probed with anti-Myc (*middle panel*) and anti-α-tubulin (*lower panel*) antibodies were used as loading controls. *B*, *in vivo* ubiquitylation assay. Western blotting of SOD1-Myc-His immunoprecipitates with anti-ubiquitin antibody demonstrated polyubiquitylation of mutant SOD1s and their C57, 146S derivatives. Replacement of Cys^6 and Cys^{111} abolished polyubiquitylation of mutant SOD1. *nr*, SOD1 without replacement in cysteine residue; *4×CS*, all four cysteines replaced by serines.

with anti-Myc antibody revealed trapped SOD1 proteins (Fig. 3*A*, *upper panel*). Interestingly, high molecular weight aggregates were abundantly detected in mutant SOD1^{G85R}, SOD1^{G93A}, and their C57S and C146S derivatives. Replacements of Cys^6 and Cys^{111} greatly reduced high molecular weight structures of mutant SOD1. No high molecular weight aggregates were present in either wild-type SOD1 or their Cys-substituted mutants.

Mutant, but not wild-type, SOD1 is conjugated to a multiubiquitin chain and degraded at the proteasome (20, 28). To assess whether SOD1 proteins are ubiquitylated, we carried out an *in vivo* ubiquitylation analysis by expressing SOD1^{WT}, SOD1^{G85R}, SOD1^{G93A}, and their Cys to Ser mutants in Neuro-2a cells in the presence of the proteasome inhibitor MG132. When SOD1 was then immunoprecipitated, mutant SOD1s, but not wild-type SOD1, were polyubiquitylated (Fig. 3*B*, *lane 1*). Replacement of both Cys^6 and Cys^{111} abolished ubiquitylation of mutant SOD1, whereas replacement of Cys^{57} and Cys^{146} did not affect the ubiquitylation status of mutant SOD1 (Fig. 3*B*, *lane 2 versus lane 3*). Wild-type SOD1 and its Cys-replacement mutants were not ubiquitylated at all. Replacing only one of the four Cys residues attenuated neither the formation of high molecular weight species nor the ubiquitylation of mutant SOD1 (data not shown). Thus, the presence of both Cys^6 and Cys^{111} is important for high molecular weight aggregate formation and ubiquitylation of mutant SOD1. Disulfide bond formation at Cys^6 or Cys^{111} is critical step for ubiquitylation of mutant SOD1.

Formation of Disulfide-linked Species of Mutant SOD1 Strongly Correlates with Visible Aggregate Formation and Neurotoxicity—Expression of mutant, but not wild-type, SOD1 induces large perinuclear intracytoplasmic aggregates in differentiated Neuro-2a cells and reduces cellular viability (20). We analyzed the role of mutant SOD1 Cys residues in aggregate formation and neurotoxicity in Neuro-2a cells. Replacements of Cys^6 and Cys^{111} significantly reduced the percentage of mutant SOD1^{G85R} and SOD1^{G93A} cells with visible aggregates (Fig. 4*A*). To further demonstrate the extent of aggregate formation, we isolated SOD1 aggregates with a procedure according to Lee *et al.* (24). Differentiated Neuro-2a cells bearing SOD1-GFP aggregates were extracted with 1% Nonidet P-40 in the culture dish, and the Nonidet P-40-soluble proteins were gently removed. Under this condition, the soluble monomeric SOD1 was completely removed, and the aggregates remained in the culture dish due to their association with unknown structures (24). The remaining Nonidet P-40-insoluble portion was then scraped and centrifuged at 80 × *g*. After the centrifugation at 80 × *g* for 15 min, the pellet fraction was found to contain exclusively the large inclusion bodies. Replacements of Cys^6 and Cys^{111} markedly reduced the number of inclusion bodies in G93A mutant SOD1-GFP (Fig. 4*B*). Mutant SOD1^{G85R} and SOD1^{G93A}, but not wild-type SOD1, are toxic in differentiated Neuro-2a cells as previously described (20). However, replacement of the Cys^6 and Cys^{111} residues markedly reduced this neurotoxicity (Fig. 4*C*), which was not affected by replacing the Cys^{57} and Cys^{146} residues. There were no significant differences among the expression levels of all the constructs (Fig. 4*D*). Thus, changes in inclusion formation and toxicity are not due to differences in altered expression. These results provide evidence of direct links among intermolecular disulfide bonding, ubiquitylated complex formation, visible aggregate formation, and neurotoxicity.

Preferential Occurrence of Disulfide-cross-linked Mutant SOD1 in the Affected Lesions of ALS Model Mice—Although mutant SOD1 is expressed at similar levels in both neuronal and non-neuronal tissues, the aggregated and ubiquitylated forms are selectively found in the pathological lesions of patients and mutant SOD1-transgenic mice (29, 30). Thus, we next examined whether mutant SOD1 is aberrantly disulfide-linked in various tissues from symptomatic mutant SOD1 transgenic mice. Western blotting analysis, using anti-SOD1 antibody under reducing and non-reducing (omitting reducing agent 2-ME) conditions, demonstrated that the expression levels of mutant SOD1 were nearly the same in all tissues examined. Each of the tissues showed some of the disulfide-linked mutant SOD1species; however, in the brain stem and spinal cord, the areas predominantly affected in mutant SOD1-linked ALS, there was increased formation of intermolecular disulfide-linked species of mutant SOD1 (Fig. 5). Thus, intermolecular disulfide-linked

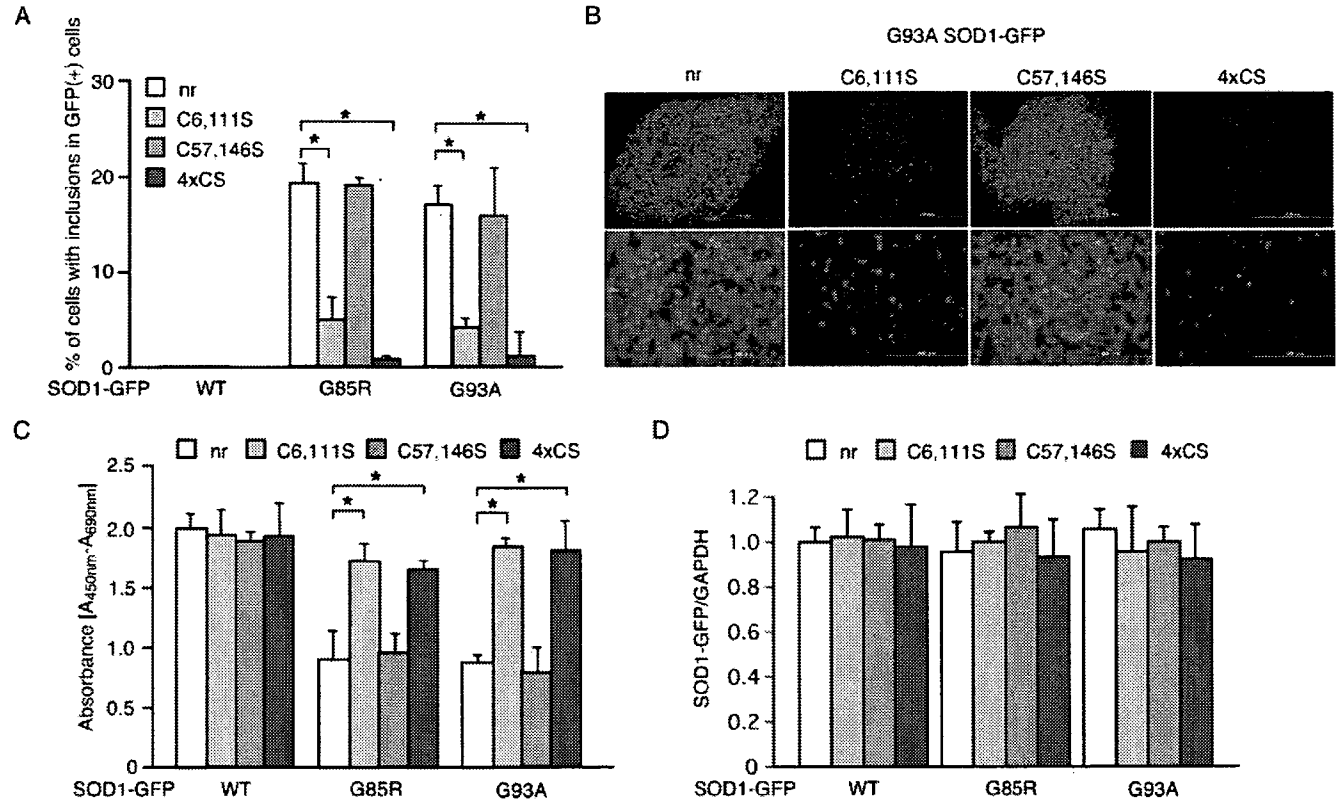

FIGURE 4. **Formation of disulfide-linked species of mutant SOD1 strongly correlates with visible aggregate formation and neurotoxicity.** *A*, the frequency of inclusion-bearing cells transfected with wild-type (*WT*), G85R, and G93A mutant SOD1-GFP and their Cys to Ser derivatives. *B*, G93A mutant SOD1-GFP inclusion bodies in 80 × *g* pellet. *Lower panels* are a high magnification image of the portion on the *upper panels* showing the whole pellet. The *scale bar* is equivalent to 10 mm in the *upper panels*, and 200 μm in the *lower panels*. *C*, change in the neurotoxic effect of mutant SOD1-GFP by Cys replacements to Ser. Cell viability was measured by the WST-1-based assay. *D*, all the constructs have equal expression. Transcription levels of SOD1-GFP in Neuro-2a cells expressing WT, G85R, and G93A mutant SOD1 and their Cys to Ser derivatives were examined by quantitative reverse transcription-PCR. Data were normalized with glyceraldehyde-3-phosphate dehydrogenase expression and then represent relative expression levels compared with levels in cells expressing WT SOD1-GFP. Data are mean ± S.D. values of triplicate assays. Statistical analyses were carried out by analysis of variance. *, $p < 0.01$. *nr*, SOD1 without replacing cysteine residues; *4×CS*, all four cysteines replaced by serines.

species are implicated as the aggregation-prone and neurotoxic intermediate of mutant SOD1 *in vivo*.

Effects of Cys^6- and Cys^{111}-mediated Disulfide Linking on the Rate of Mutant SOD1 Degradation—To determine whether replacement of Cys residues affects the degradation of SOD1 proteins, we examined the stability of mutant SOD1 proteins expressed in Neuro-2a cells (Fig. 6, *A* and *B*). Chase experiments with cycloheximide, which halts all cellular protein synthesis, demonstrated that replacement of Cys residues did not influence the stability of wild-type SOD1 protein (Fig. 6*A*). By contrast, although mutant SOD1 showed the enhanced degradation compared with wild-type proteins previously described (18–20), when both Cys^6 and Cys^{111} were replaced with Ser, the degradation of mutant SOD1 was markedly increased (Fig. 6*B*). Replacement of Cys^{57} and Cys^{146} did not significantly change the rate of degradation compared with Cys-native mutant SOD1 protein.

Ubiquityl Ligase Dorfin Ubiquitylates and Promotes Degradation of Disulfide-linked Mutant SOD1—We have previously shown that Dorfin physically binds and ubiquitylates various familial ALS-linked SOD1 mutants and enhances their degradation (20). Thus, we examined whether Cys residues on SOD1 affect the binding and ubiquitylating activities of Dorfin. To this end, Dorfin was co-expressed with wild-type or mutant SOD1 in Neuro-2a cells. Dorfin co-immunoprecipitated with G85R and G93A mutant SOD1s and their Cys^{57}- and Cys^{146}-replaced derivatives (Fig. 7*A*). However, Dorfin interacted with Cys^6- and Cys^{111}-replaced mutant SOD1 only very weakly and failed to bind to mutant SOD1 when all four Cys residues were replaced (Fig. 7*A*). Dorfin did not bind at all to wild-type SOD1. Using an *in vivo* ubiquitylation assay, we further examined whether co-expressed Dorfin enhances the ubiquitylation of Cys-substituted mutant SOD1 (Fig. 7*B*). When Cys-native or Cys^{57}- and Cys^{146}-replaced mutant SOD1s were co-expressed with Dorfin, ubiquitylation of mutant SOD1s were increased; however, co-expression of Dorfin with mutant SOD1 in which Cys^6 and Cys^{111} or all four Cys residues were replaced did not promote ubiquitylation of these mutant SOD1s (Fig. 7*B*). Chase experiments with cycloheximide in the presence or absence of Dorfin demonstrated that degradation of Cys-native and Cys^{57}- and Cys^{146}-replaced mutant SOD1^{G93A} was greatly accelerated when Dorfin was overexpressed, whereas the stability of Cys^6 and Cys^{111} or all four Cys-replaced mutant SOD1G93A were unaffected (Fig. 7*C*). We have previously shown that Dorfin exerts neuroprotective effects by promoting degradation of mutant SOD1 through its ubiquityl ligase activities (20). Co-expression of Dorfin improved the viability of Neuro-2a cells expressing Cys-

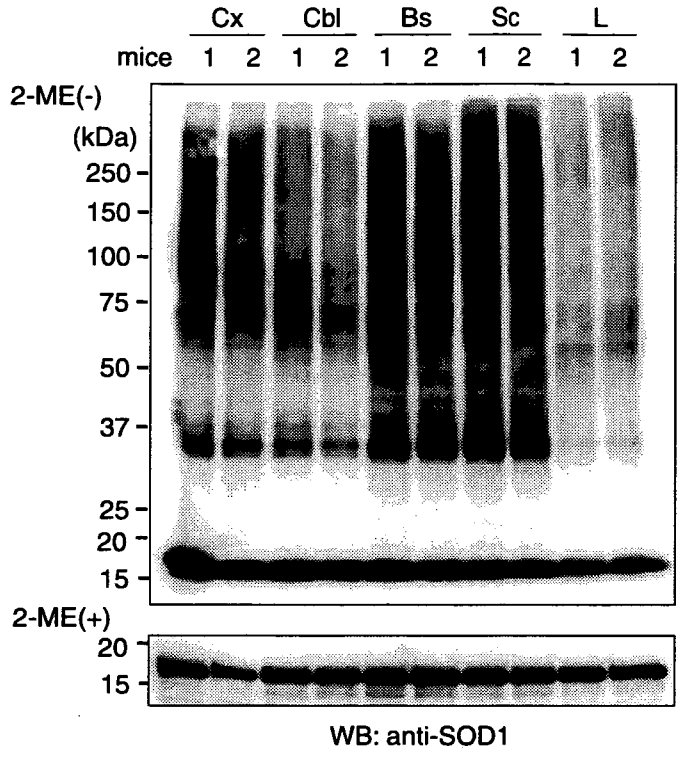

FIGURE 5. **Preferential occurrence of disulfide-cross-linked mutant SOD1 in the affected lesion of ALS model mice.** Western blotting of tissue samples from two 17-week-old symptomatic G93A mutant SOD1-transgenic mice under non-reducing (*upper panel*) and reducing (*lower panel*) conditions. *Cx*, cerebral cortex; *Cbl*, cerebellum; *Bs*, brain stem; *Sc*, spinal cord; *L*, liver.

native and Cys^{57}- and Cys^{146}-replaced mutant $SOD1^{G93A}$ (Fig. 7*D*).

DISCUSSION

Mutations in the *SOD1* gene cause familial ALS through the gain of a toxic function, however, the nature of this toxic function remains largely unknown (31). Ubiquitylated aggregates of mutant SOD1 proteins in affected lesions are a pathological hallmark of the disease (32) and suggest their relation to neurotoxicity. Recent biochemical studies suggest that the immature disulfide-reduced forms of the familial ALS mutant SOD1 proteins play a critical role in this neurotoxicity; *in vitro*, these forms tend to misfold, oligomerize, and readily undergo incorrect disulfide bond formation upon mild oxidative stress (16, 33). Among the more than 100 ALS-associated human SOD1 mutants, some cannot intrinsically form the essential intramolecular disulfide bonds. One of the conserved Cys residues, Cys^{146}, is missing in some of the mutants, such as the Leu^{126} del TT (stop at 131) and Gly^{127} ins TGGG (stop at 133); however, it has been reported that minute quantities of SOD1 aggregates can cause the disease in mice expressing the truncated mutant, Gly^{127} ins TGGG (stop at 133) (34). Furthermore, a significant fraction of the insoluble SOD1 aggregates in the spinal cord of ALS model mice contain multimers cross-linked via intermolecular disulfide bonds (17, 35). In the present study, we showed that non-physiological intermolecular disulfide bonds involving Cys^{6} and Cys^{111} of the mutant SOD1 were important for high molecular weight aggregate formation, ubiquitylation, and neurotoxicity *in vivo*, all of which were dramatically reduced in Neuro-2a cells when these residues were replaced with serines.

Human SOD1 has two free cysteine residues, Cys^{6} and Cys^{111} (36). Cys^{6} is located adjacent to the dimer interface pointed toward the interior of the β-barrel and is solute-inaccessible in the native, folded conformation. Cys^{111} is located near the surface and is solute-accessible and -reactive, often becoming blocked during purification (37). Replacement of the free Cys residues increased the resistance to thermal inactivation (38). Increased resistance of mutant SOD1s is due to increased resistance to irreversible unfolding and relatively unaffected by changes in conformational stability (39). Our data, showing that aggregate formation of mutant SOD1 is reduced when Cys^{6} and Cys^{111} are replaced with serines, are compatible with these observations. Mutations of the Cys^{6} residue (C6F and C6G) still result in familial ALS (4), and in a transgenic mouse expressing mouse SOD1 retaining cystines 6, 57, and 146 but lacking

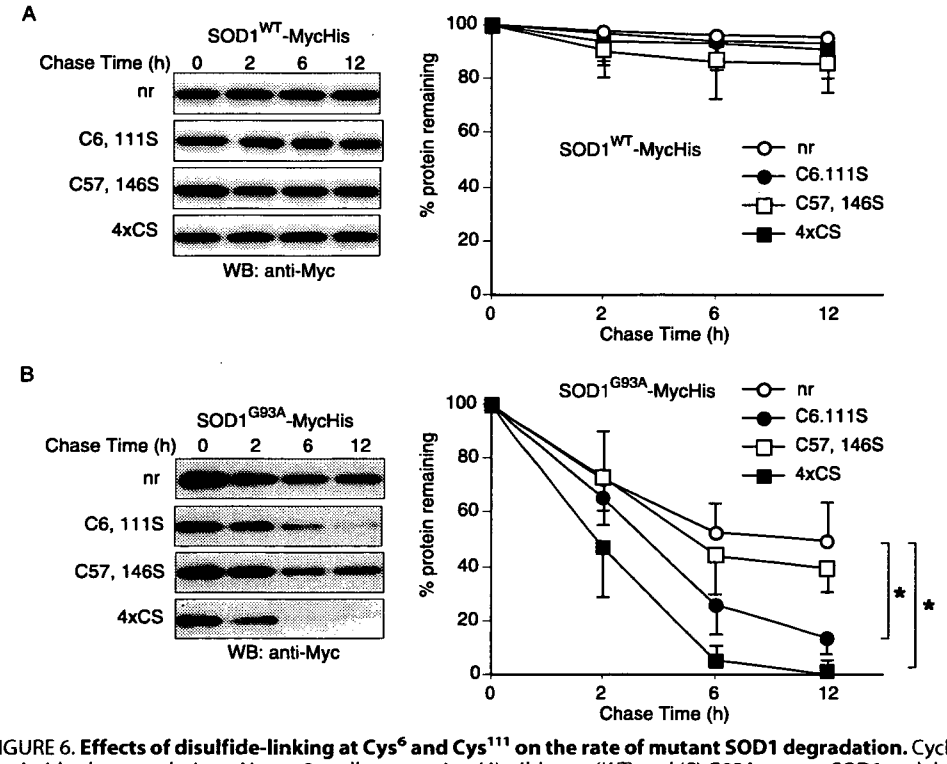

FIGURE 6. **Effects of disulfide-linking at Cys^{6} and Cys^{111} on the rate of mutant SOD1 degradation.** Cycloheximide chase analysis on Neuro-2a cells expressing (*A*) wild-type (*WT*) and (*B*) G93A mutant SOD1 and their Cys to Ser derivatives. Western blots showing levels of SOD1 protein at various times after the cycloheximide chase are in the *left panels*. Quantitative data on the right are mean ± S.D. values of three independent experiments. Statistical analyses were carried out by analysis of variance. *, $p < 0.01$. *nr*, SOD1 without cysteine residue replacement; *4×CS*, all four cysteines replaced by serines.

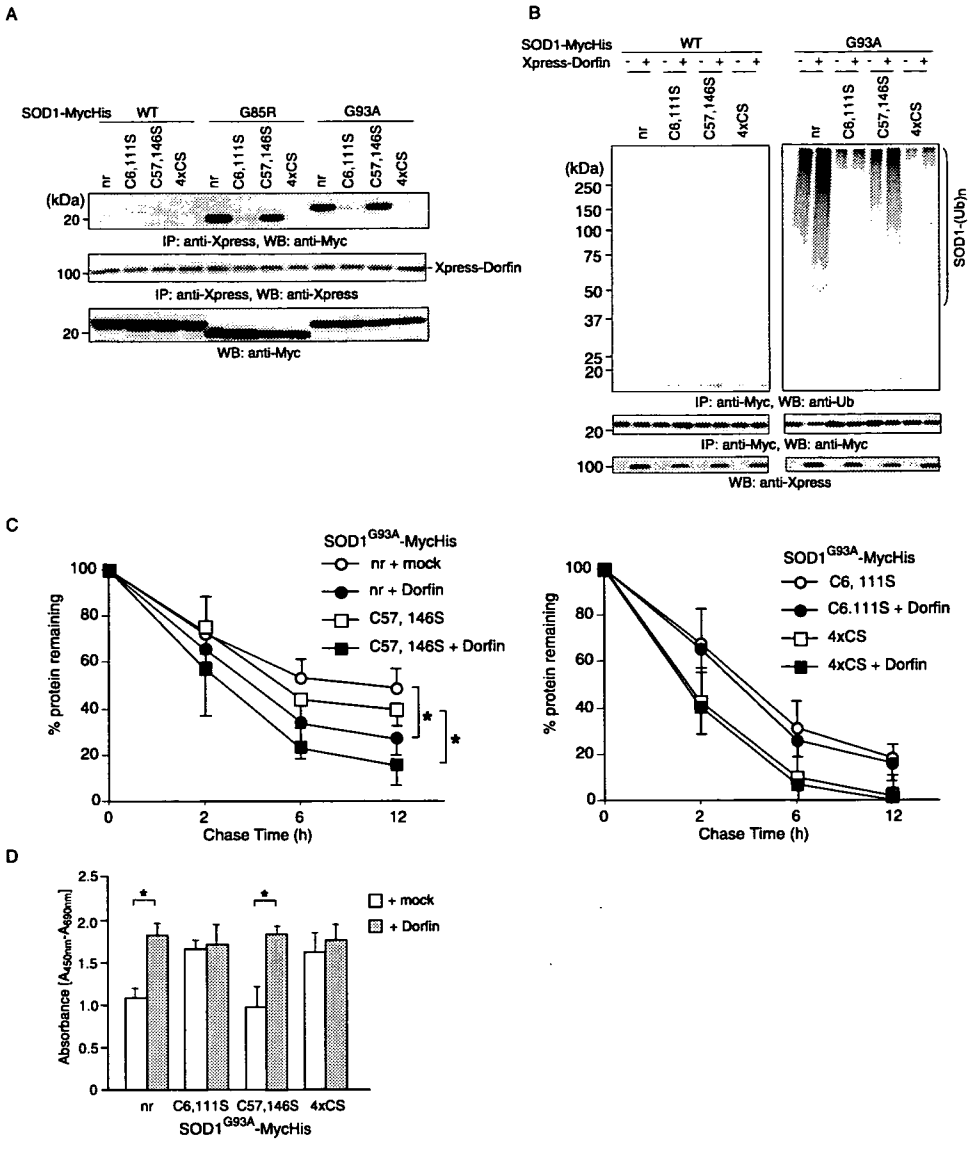

FIGURE 7. **Ubiquityl ligase Dorfin binds, ubiquitylates, and promotes degradation of disulfide-linked mutant SOD1.** *A*, replacement of Cys^6 and Cys^{111} nearly eliminated the interaction of Dorfin with mutant SOD1. Various SOD1-MycHis were co-transfected with Xpress-Dorfin. After immunoprecipitation with anti-Xpress antibody, the resulting precipitates and cell lysates were analyzed by Western blotting with anti-Myc antibody. *B, in vivo*, Dorfin failed to promote ubiquitylation of mutant SOD1 with the Cys^6 and Cys^{111} replacement. Western blotting of SOD1-Myc-His immunoprecipitates with anti-ubiquitin antibody. *C*, Dorfin failed to promote degradation of mutant SOD1 with both Cys^6 and Cys^{111} replaced. Cycloheximide chase analysis of G93A mutant SOD1 with Cys^6 and Cys^{111}-replacements (*left panel*) or with Cys^{57} and Cys^{146}-replacements (*right panel*) in the presence or absence of overexpressed Xpress-Dorfin. *D*, Dorfin prevented neurotoxicity by mutant SOD1 with intact Cys^6 and Cys^{111} residues. Cell viability was measured by the WST-1-based assay. Data are mean ± S.D. values of three independent experiments. Statistical analyses were carried out by unpaired *t* test. *, $p < 0.01$. *nr*, SOD1 without replacement in cysteine residue; *4×CS*, all four cysteines replaced by serines.

111 and with a G86R mutation corresponding to G85R mutation in human SOD1, degeneration of motor neurons in the spinal cord has been observed (40). These results imply that, if one of either the Cys^6 or Cys^{111} residues is present, it can still be a disease-causing SOD1. Our data here also revealed that replacement of only one of the Cys residues at positions 6 or 111 had modest effects on the formation of aggregates (Fig. 2).

Cytoplasmic proteins are degraded mainly via two pathways, the ubiquitin-proteasome pathway (6) and via autophagy (7). Previous studies have shown that mutant SOD1 proteins are turned over more rapidly than wild-type SOD1 (12, 18, 19). Two distinct ubiquitin ligases, Dorfin and NEDL1, were reported to specifically ubiquitylate mutant but not wild-type SOD1 (20, 21). These studies suggest that mutant SOD1 is degraded by the ubiquitin-proteasome pathway and that the accelerated turnover of mutant SOD1 is mediated in part by this pathway. Impairment of the proteasome activities may contribute to ALS pathogenesis (28, 41, 42). We showed here that proteasome inhibition led to a dose-dependent accumulation of aberrant disulfide-linked high molecular weight mutant SOD1 (Fig. 1), suggesting that disulfide-linking mediates ubiquitylation of mutant SOD1. In fact, we found that Dorfin ubiquitylated mutant SOD1 by recognizing the Cys^6 and Cys^{111} disulfide cross-linked form and targeted it for proteasomal degradation (Fig. 7). Mutant SOD1, in which the Cys^6 and Cys^{111} were replaced, was not ubiquitylated (Fig. 3), and its rate of degradation was not affected in the presence of Dorfin (Fig. 7). It is possible that mutant SOD1 lacking Cys^6 and Cys^{111} may be degraded directly by the proteasome without ubiquitylation (43) or by autophagy (44), but further studies are needed to address this issue.

The appearance of mutant SOD1 aggregates in motor neurons of familial ALS patients and mouse models has suggested that aggregation plays an important role in neurotoxicity (31). However, conflicting results have been reported on the correlation between aggregate formation and cell death. One report showed that aggregate formation of mutant $SOD1^{A4V}$ and $SOD1^{V148G}$ does not correlate with cell death (45), whereas another study using live cell-imaging techniques reported that the ability of mutant $SOD1^{G85R}$ and $SOD1^{G93A}$ proteins to form aggregates directly correlates with neuronal cell death (46). These controversies also exist in other neurodegenerative diseases (47, 48). In this study, we clearly showed a direct link among intermolecular disulfide bond-mediated high molecular weight complex formation, visible aggregate formation, and neurotoxicity (Figs. 2–4).

Furukawa *et al.* (16) reported that formation of disulfide-linked multimers need not involve the non-conserved Cys residues, Cys^6 and Cys^{111}, and that the conserved Cys residues, Cys^{57} and Cys^{146}, play an important role in the apo-form of

SOD1 multimerization upon oxidative stress. Our results underscore the importance of Cys^{6} and Cys^{111} for high molecular weight aggregate formation, ubiquitylation, and neurotoxicity in Neuro-2a cells. This discrepancy may result from differences in experimental conditions; we studied human SOD1 proteins expressed in Neuro-2a cells, and Furukawa *et al.* used the purified apo-form of human SOD1 from *Escherichia coli*. Further studies will clarify the roles of each of the Cys residues of the mutant SOD1 protein in the ALS pathogenesis *in vivo* by generating transgenic mice bearing mutant SOD1 lacking Cys^{6} and Cys^{111} or Cys^{57} and Cys^{146}.

REFERENCES

1. McCord, J. M., and Fridovich, I. (1969) *J. Biol. Chem.* **244,** 6049–6055
2. Fridovich, I. (1974) *Adv. Enzymol. Relat. Areas. Mol. Biol.* **41,** 35–97
3. Rosen, D. R. (1993) *Nature* **364,** 362
4. Valentine, J. S., Doucette, P. A., and Potter, S. Z. (2005) *Annu. Rev. Biochem.* **74,** 563–593
5. Crapo, J. D., Oury, T., Rabouille, C., Slot, J. W., and Chang, L. Y. (1992) *Proc. Natl. Acad. Sci. U. S. A.* **89,** 10405–10409
6. Fridovich, I. (1986) *Adv. Enzymol. Relat. Areas. Mol. Biol.* **58,** 61–97
7. Fisher, C. L., Cabelli, D. E., Tainer, J. A., Hallewell, R. A., and Getzoff, E. D. (1994) *Proteins* **19,** 24–34
8. Arnesano, F., Banci, L., Bertini, I., Martinelli, M., Furukawa, Y., and O'Halloran, T. V. (2004) *J. Biol. Chem.* **279,** 47998–48003
9. Freedman, R. B. (1995) *Curr. Opin. Struct. Biol.* **5,** 85–91
10. Lindenau, J., Noack, H., Possel, H., Asayama, K., and Wolf, G. (2000) *Glia* **29,** 25–34
11. Tiwari, A., and Hayward, L. J. (2003) *J. Biol. Chem.* **278,** 5984–5992
12. Borchelt, D. R., Lee, M. K., Slunt, H. S., Guarnieri, M., Xu, Z. S., Wong, P. C., Brown, R. H., Jr., Price, D. L., Sisodia, S. S., and Cleveland, D. W. (1994) *Proc. Natl. Acad. Sci. U. S. A.* **91,** 8292–8296
13. Ratovitski, T., Corson, L. B., Strain, J., Wong, P., Cleveland, D. W., Culotta, V. C., and Borchelt, D. R. (1999) *Hum. Mol. Genet* **8,** 1451–1460
14. Rakhit, R., Crow, J. P., Lepock, J. R., Kondejewski, L. H., Cashman, N. R., and Chakrabartty, A. (2004) *J. Biol. Chem.* **279,** 15499–15504
15. Doucette, P. A., Whitson, L. J., Cao, X., Schirf, V., Demeler, B., Valentine, J. S., Hansen, J. C., and Hart, P. J. (2004) *J. Biol. Chem.* **279,** 54558–54566
16. Furukawa, Y., and O'Halloran, T. V. (2005) *J. Biol. Chem.* **280,** 17266–17274
17. Furukawa, Y., Fu, R., Deng, H. X., Siddique, T., and O'Halloran, T. V. (2006) *Proc. Natl. Acad. Sci. U. S. A.* **103,** 7148–7153
18. Hoffman, E. K., Wilcox, H. M., Scott, R. W., and Siman, R. (1996) *J. Neurol. Sci.* **139,** 15–20
19. Johnston, J. A., Dalton, M. J., Gurney, M. E., and Kopito, R. R. (2000) *Proc. Natl. Acad. Sci. U. S. A.* **97,** 12571–12576
20. Niwa, J., Ishigaki, S., Hishikawa, N., Yamamoto, M., Doyu, M., Murata, S., Tanaka, K., Taniguchi, N., and Sobue, G. (2002) *J. Biol. Chem.* **277,** 36793–36798
21. Miyazaki, K., Fujita, T., Ozaki, T., Kato, C., Kurose, Y., Sakamoto, M., Kato, S., Goto, T., Itoyama, Y., Aoki, M., and Nakagawara, A. (2004) *J. Biol. Chem.* **279,** 11327–11335
22. Niwa, J., Ishigaki, S., Doyu, M., Suzuki, T., Tanaka, K., and Sobue, G. (2001) *Biochem. Biophys. Res. Commun.* **281,** 706–713
23. Marin, I., and Ferrus, A. (2002) *Mol. Biol. Evol.* **19,** 2039–2050
24. Lee, H. J., and Lee, S. J. (2002) *J. Biol. Chem.* **277,** 48976–48983
25. Scherzinger, E., Lurz, R., Turmaine, M., Mangiarini, L., Hollenbach, B., Hasenbank, R., Bates, G. P., Davies, S. W., Lehrach, H., and Wanker, E. E. (1997) *Cell* **90,** 549–558
26. Bailey, C. K., Andriola, I. F., Kampinga, H. H., and Merry, D. E. (2002) *Hum. Mol. Genet.* **11,** 515–523
27. Wang, J., Xu, G., and Borchelt, D. R. (2002) *Neurobiol. Dis.* **9,** 139–148
28. Urushitani, M., Kurisu, J., Tsukita, K., and Takahashi, R. (2002) *J. Neurochem.* **83,** 1030–1042
29. Gurney, M. E., Pu, H., Chiu, A. Y., Dal Canto, M. C., Polchow, C. Y., Alexander, D. D., Caliendo, J., Hentati, A., Kwon, Y. W., Deng, H. X., Chen, W., Zhai, P., Sufit, R. L., and Siddique, T. (1994) *Science* **264,** 1772–1775
30. Bruijn, L. I., Houseweart, M. K., Kato, S., Anderson, K. L., Anderson, S. D., Ohama, E., Reaume, A. G., Scott, R. W., and Cleveland, D. W. (1998) *Science* **281,** 1851–1854
31. Cleveland, D. W., and Rothstein, J. D. (2001) *Nat. Rev. Neurosci.* **2,** 806–819
32. Watanabe, M., Dykes-Hoberg, M., Culotta, V. C., Price, D. L., Wong, P. C., and Rothstein, J. D. (2001) *Neurobiol. Dis.* **8,** 933–941
33. Wang, J., Xu, G., and Borchelt, D. R. (2006) *J. Neurochem.* **96,** 1277–1288
34. Jonsson, P. A., Graffmo, K. S., Andersen, P. M., Brannstrom, T., Lindberg, M., Oliveberg, M., and Marklund, S. L. (2006) *Brain* **129,** 451–464
35. Deng, H. X., Shi, Y., Furukawa, Y., Zhai, H., Fu, R., Liu, E., Gorrie, G. H., Khan, M. S., Hung, W. Y., Bigio, E. H., Lukas, T., Dal Canto, M. C., O'Halloran, T. V., and Siddique, T. (2006) *Proc. Natl. Acad. Sci. U. S. A.* **103,** 7142–7147
36. Getzoff, E. D., Tainer, J. A., Stempien, M. M., Bell, G. I., and Hallewell, R. A. (1989) *Proteins* **5,** 322–336
37. Briggs, R. G., and Fee, J. A. (1978) *Biochim. Biophys. Acta* **537,** 86–99
38. McRee, D. E., Redford, S. M., Getzoff, E. D., Lepock, J. R., Hallewell, R. A., and Tainer, J. A. (1990) *J. Biol. Chem.* **265,** 14234–14241
39. Lepock, J. R., Frey, H. E., and Hallewell, R. A. (1990) *J. Biol. Chem.* **265,** 21612–21618
40. Ripps, M. E., Huntley, G. W., Hof, P. R., Morrison, J. H., and Gordon, J. W. (1995) *Proc. Natl. Acad. Sci. U. S. A.* **92,** 689–693
41. Kabashi, E., Agar, J. N., Taylor, D. M., Minotti, S., and Durham, H. D. (2004) *J. Neurochem.* **89,** 1325–1335
42. Cheroni, C., Peviani, M., Cascio, P., Debiasi, S., Monti, C., and Bendotti, C. (2005) *Neurobiol. Dis.* **18,** 509–522
43. Di Noto, L., Whitson, L. J., Cao, X., Hart, P. J., and Levine, R. L. (2005) *J. Biol. Chem.* **280,** 39907–39913
44. Kabuta, T., Suzuki, Y., and Wada, K. (2006) *J. Biol. Chem.* **281,** 30524–30533
45. Lee, J. P., Gerin, C., Bindokas, V. P., Miller, R., Ghadge, G., and Roos, R. P. (2002) *J. Neurochem.* **82,** 1229–1238
46. Matsumoto, G., Stojanovic, A., Holmberg, C. I., Kim, S., and Morimoto, R. I. (2005) *J. Cell Biol.* **171,** 75–85
47. Arrasate, M., Mitra, S., Schweitzer, E. S., Segal, M. R., and Finkbeiner, S. (2004) *Nature* **431,** 805–810
48. Saudou, F., Finkbeiner, S., Devys, D., and Greenberg, M. E. (1998) *Cell* **95,** 55–66

Ataxic vs painful form of paraneoplastic neuropathy

Y. Oki, MD
H. Koike, MD
M. Iijima, MD
K. Mori, MD
N. Hattori, MD
M. Katsuno, MD
T. Nakamura, MD
M. Hirayama, MD
F. Tanaka, MD
M. Shiraishi, MD
S. Yazaki, MD
K. Nokura, MD
H. Yamamoto, MD
G. Sobue, MD

CME

Address correspondence and reprint requests to Dr. Gen Sobue, Department of Neurology, Nagoya University, Graduate School of Medicine, Nagoya 466-8550 Japan
sobueg@med.nagoya-u.ac.jp

ABSTRACT

Objective: To characterize the clinicopathologic features of ataxic and painful forms of paraneoplastic neuropathy.

Methods: Clinical, electrophysiologic, and histopathologic findings were assessed in 17 patients with paraneoplastic neuropathy.

Results: Clinical features can be categorized into two groups: one group (13 patients) with predominantly deep sensory disturbance and a second group (4 patients) with predominantly superficial sensory disturbance. The former group showed severe sensory ataxia and predominantly large myelinated fiber loss in the sural nerve. The latter group showed marked pain, in particular, severe mechanical hyperalgesia, and predominantly small myelinated and unmyelinated fiber loss. Nerve conduction assessment indicated an axonal neuropathy pattern in both groups, while sensory action potentials were more markedly diminished in the sensory ataxic form. Anti-Hu antibodies were detected in half of the patients in both groups. Treatment for cancer was effective to improve or stabilize neuropathic symptoms in some cases from both groups. Immunotherapy was effective only for a short time.

Conclusions: Paraneoplastic neuropathy can be characterized into two groups by the presence of sensory ataxia or severe spontaneous pain and severe mechanical hyperalgesia. Preferential small myelinated and unmyelinated fiber loss correlated to the cases of severe pain.
***Neurology*® 2007;69:564-572**

Paraneoplastic neurologic disorders are a rare group of syndromes that occur in patients with cancer and are not due to the presence of metastasis or direct infiltration of the cancer into the nervous system.[1-3] They comprise a number of different clinicopathologic entities such as paraneoplastic neuropathy, paraneoplastic encephalomyelitis, paraneoplastic cerebellar degeneration, and limbic encephalitis.[3,4]

Paraneoplastic neuropathy is one of the most frequent paraneoplastic neurologic diseases, and is most commonly associated with lung small cell cancer.[5-7] The typical clinical course is characterized as subacute onset, with dysesthesias, a wide ranged sensory impairment particularly of the kinesthetic sensation leading to sensory ataxia.[4,5,8] Motor function is preserved or only modestly impaired.[8] Neurologic symptoms often occur before the cancer is detected.[4-6] The primary responsible lesion of paraneoplastic neuropathy has been considered to be the impairment of sensory neuronal cell bodies in the dorsal root ganglia (DRG), probably due to the involvement of the cellular immune system.[9] Morphometric studies at autopsy showed a preferential loss of large-diameter sensory neurons, a marked decrease in large myelinated fibers in the dorsal root and sural nerve, and a severe loss of myelinated fibers in the fasciculus gracilis.[10,11]

The definite diagnosis of this disease at an early stage and the immediate application of

Supplemental data at www.neurology.org

From the Department of Neurology (Y.O., H.K., M.I., K.M., N.H., M.K., T.N., M.H., F.T., M.S.), Nagoya University Graduate School of Medicine; Department of Neurology (M.S.), Kawasaki Municipal Tama Hospital; Department of Neurology (S.Y.), St. Marianna University School of Medicine, Yokohama City Seibu Hospital, Kawasaki; and Department of Neurology (K.N., H.Y.), Fujita Health University, Banbuntane Hotokukai Hospital, Nagoya, Japan.

Supported by grants from the Ministry of Labor, Welfare and Health of Japan.

Disclosure: The authors report no conflicts of interest.

Table 1 Neuropathic symptoms

Patient	Age, y/sex	Initial symptoms	Progression, mo	Distribution of sensory signs	Sensory signs: Spontaneous pain	Pain*	Vibration	Position	Romberg sign/ataxia	Muscle weakness/ atrophy	MRS
Ataxic form											
1	70/F	Numbness, U, L	6	Symmetrical	+1	−2	−3	−3	+/+3	−	4
2	61/M	Numbness, L	3	Multifocal	+1	−2	−3	−3	+/+3	−	4
3	67/M	Paresthesia, L	7	Symmetrical	+1	−1	−3	−3	+/+3	−	4
4	71/M	Numbness, U	6	Multifocal	+1	−2	−3	−3	+/+3	−	4
5	61/M	Numbness, U	2	Multifocal	−	+1	−3	−3	+/+2	+1	3
6	65/M	Numbness, L	1	Symmetrical	−	−1	−3	−3	+/+3	−	4
7	75/M	Gait disturbance	3	Symmetrical	−	−1	−3	−3	+/+3	−	4
8	64/F	Numbness, L	3	Multifocal	−	−1	−3	−3	+/+2	+1	3
9	65/M	Numbness, L	1.5	Symmetrical	+1	−	−3	−3	+/+3	+2	4
10	54/M	Numbness, L	2	Multifocal	+1	−2	−3	−3	+/+2	+1	3
11	71/F	Numbness, U	6	Multifocal	+1	−1	−3	−3	+/+2	+1	3
12	76/M	Numbness, U, L	4	Multifocal	−	−	−3	−2	+/+3	+1	4
13	49/M	Numbness, U	2	Multifocal	+1	−1	−3	−3	+/+2	−	2
Painful form											
14	66/M	Pain, L	7	Symmetrical	+3	+2	−3	−	−	−	2
15	63/M	Numbness, U	6	Multifocal	+3	+2	−3	−2	+/+1	+1	4
16	72/F	Numbness, U	1	Multifocal	+3	+3	−1	−	−	+1	4
17	67/F	Pain, L	3	Multifocal	+3	+2	−1	−	−	+1	3

Sensory signs were evaluated in the distal portion of the arms or the legs. Distribution of sensory signs: U = upper extremity, L = lower extremity. +1, +2, and +3 represent mild, moderate, and severe degree of sensory signs, ataxia, and muscle weakness. −1, −2, and −3 represent mild, moderate, and severe reduction for sensory signs.
*Pain is divided into two categories: hyperalgesia (+1, +2, or +3) and hypoalgesia (−1, −2, or −3).
MRS = modified Rankin scale[21] (0, asymptomatic; 1, nondisabling symptoms not interfering with lifestyle; 2, minor disability from symptoms leading to some restriction of lifestyle but not interfering with patients' capacity to look after themselves; 3, moderate disability from symptoms significantly interfering with lifestyle or preventing totally independent existence; 4, moderately severe disability from symptoms clearly precluding independent existence, though not requiring 24-hour attention from a caregiver; and 5, severe disability and total dependence, requiring constant attention day and night); + = positive findings; − = negative findings.

therapy for cancer are significant.[6,12] Although the diagnostic usefulness of onconeural antibodies associated with this disease is widely recognized,[13-15] the definite diagnosis was difficult due to the existence of many cases that lack onconeural antibodies and to the wide clinical spectrum.[15,16] Clarification of the clinical spectrum is necessary for early diagnosis.

Patients with sensory symptoms characterized as pain and painful dysesthesia or mechanical hyperalgesia have been recognized only anecdotally.[5,8] The symptoms and underlying pathology of paraneoplastic sensory neuropathy may be more broad than has been recognized, and are not restricted to sensory ataxia-predominant neuropathy.

In the present report we review the clinicopathologic features of 17 patients with paraneoplastic neuropathy, and describe a painful form with characteristic pathologic features.

METHODS The subjects consisted of 12 men and 5 women ranging from 49 to 76 years of age (mean age ± SD, 65.7 ± 7.0 years) who were referred to Nagoya University Hospital and its affiliated institutions between 1988 and 2004 (table 1). Fifteen of the patients (Patients 1, 3 to 14, 16, and 17) were referred for the first time due to neuropathic symptoms, and the presence of cancer was not diagnosed at the time of first referral. Another two patients (Patients 2 and 15) were diagnosed with cancer before neurologic symptoms appeared and one of them (Patient 15) had received

chemotherapy. However, the chemotherapy ended within 1 year of the cancer diagnosis in this patient and no neurologic symptoms were observed throughout the period and for the subsequent 2.5 years. A recurrence of cancer was detected 6 months after the appearance of the neurologic symptoms. Except for this patient, no treatments for cancer were performed before the appearance of neurologic symptoms. We examined all patients carefully to determine that the neuropathies were not caused by the direct invasion of cancers, and other known causes of neuropathies, including diabetes mellitus, renal failure, vitamin deficiency, thyroid dysfunction, paraproteinemias, cachexia, and autoimmune disease, were excluded from the study. Recently, Graus et al. proposed diagnostic criteria for paraneoplastic neurologic syndromes, and suggested two levels of evidence to define a neurologic syndrome as paraneoplastic: "definite" and "possible".[3] Details of the criteria are described in table E-1 on the *Neurology* Web site at www.neurology.org. According to the criteria, 15 of our patients (Patients 1 to 15) met one of the criteria for "definite." As for the other two patients (Patients 16 and 17), they were included as having possible paraneoplastic neurologic syndromes according to the "possible" criteria 3. The subjects underwent general physical and neurologic examinations, routine blood and urine studies, CSF analysis, nerve conduction studies, and sural nerve biopsies. The deep sensory disturbances were assessed by vibration sense and joint position sense, and superficial sensory disturbances were assessed by pin-prick stimulation or gently touching the skin. Autonomic symptoms were assessed by examining or interviewing patients, or reviewing the clinical records, and clinically in the terms of the presence or absence of urinary retention, constipation, and orthostatic hypotension. The patients' sera and/or CSF were assessed for the presence of well-characterized onconeural antibodies.[3,14] The evaluation of onconeural antibodies was performed at the Mayo Medical Laboratories, USA.[17-20] Anti-Hu, anti-Ri, ANNA-3, anti-Yo, PCA-2, anti-Tr, anti-CV2, and amphiphysin antibodies were assessed by an indirect immunofluorescence assay, the details of which were described previously.[17-20] Activities of daily living (ADL) were evaluated by a modified Rankin scale.[21] We considered the treatment effective if there was at least a one-point improvement in the Rankin scale.[22] In addition, we considered the treatment effective when the progression of clinical symptoms was stabilized due to the treatment.

Motor and sensory conduction was measured in the median, tibial, and sural nerves, using a standard method with surface electrodes for stimulation and recording.[23,24] Motor conduction was investigated in the median and tibial nerves, by recording from the abductor pollicis brevis and abductor hallucis brevis muscles. Sensory conduction in the median and sural nerves was recorded at the second digit with ring electrodes and at the ankle, as described previously.[23,24]

A sural nerve biopsy was performed in all patients as described previously.[25-28] Specimens were divided into two portions. The first of these was fixed in 2.5% glutaraldehyde in 0.125 M cacodylate buffer (pH 7.4) and embedded in epoxy resin for morphometric and ultrastructural examination. The density of myelinated fibers was assessed in toluidine blue-stained semithin sections using a computer-assisted image analyzer (Luzex FS; Nikon, Tokyo, Japan), and the densities of small and large myelinated fibers were calculated as described previously.[25-28]

For electron microscopic analysis, epoxy resin-embedded specimens were cut into ultrathin transverse sections and stained with uranyl acetate and lead citrate. To assess the density of unmyelinated fibers, electron microscopic photographs were taken at a magnification of ×4000 in a random fashion to cover the ultrathin sections, as described previously.[25,27,28] The density of unmyelinated fibers was estimated from these electron micrographs. A fraction of the glutaraldehyde-fixed sample was processed for a teased-fiber study, in which at least 100 single fibers were isolated and their pathologic condition was assessed microscopically according to criteria described previously.[25,29,30]

The second portion of the specimen was fixed in 10% formalin solution and embedded in paraffin. Sections were cut by routine methods and stained with hematoxylin and eosin, as well as by the Klüver-Barrera and Masson trichrome methods.

Quantitative data are presented as the mean ± SD with or without an accompanying range, and compared with our control values.[25,31-33] Statistical analyses were performed using the χ^2 test or the Wilcoxon rank sum test as appropriate. p Values less than 0.05 were considered to indicate significance.

RESULTS Clinical features of paraneoplastic neuropathy: Ataxic and painful forms. The initial neurologic symptom was numbness of the limbs in 13 patients, pain of the limbs in 2 patients, gait disturbance in 1 patient, and paresthesia of the lower limb in 1 patient. Six patients showed apparent laterality and 8 patients showed involvement of the upper limbs at initial phase. Progression of symptoms was acute within 1 month in 2 patients, subacute within 1 month to 6 months in 13 patients, and chronic after more than 6 months in 2 patients. Sensory signs were distributed in a symmetric polyneuropathy pattern in 6 patients (35%) and in a mononeuritis multiplex pattern in 11 patients (65%). Sensory symptoms were distributed over the limbs in all patients and the trunk in 2 patients, but were not present in the face in any patient. There were no symptoms suggesting CNS involvement in any of the patients.

According to the features of sensory symptoms, we can categorize the patients into two groups. One group consisting of 13 patients showed predominantly deep sensory disturbance particularly with kinesthetic sensory impairment. All of the patients in this group showed positive Romberg sign and severe sensory ataxia (table 1). Eight patients of this group reported spontaneous pain, but their pain was not the predominant symptom. The other group consisted of 4 patients who had severe spontaneous pain and mechanical hyperalgesia, defined by provocation or exacerbation of painful sensation by pinprick stimulation (i.e., pinprick hyperalgesia) or gentle tactile stimulation (i.e., allodynia). In this group, mild deep sensory disturbance inducing sensory ataxia

Table 2 Details of associated cancer, onconeural antibodies, CSF, and treatments

Patient	From neurologic onset to cancer diagnosis, mo	Cancer	Onconeural antibodies	CSF cell (/mm^3)/ protein (mg/dL)	Treatment
Ataxic form					
1	10	SCLC	Hu	ND	C*, R*
2	−7	SCLC	Hu, CV2	ND	Ope, C
3	8	Gastric (adeno)	Hu	2/40	Ope
4	9	SCLC	Hu	10/160	C
5	5	SCLC	Hu	4/103	C, St, IVIg*, PE*
6	5	SCLC	Hu	53/596	C
7	8	Gastric (adeno)	–	2/49	None
8	8	Non-SCLC (large cell)	–	ND	Ope*
9	3	Small cell mediastinal	–	3/92	C
10	1	Non-SCLC (adeno)	–	ND	R
11	20	SCLC	–	1/49	St, IvIg
12	18	Adenocarcinoma†	–	13/102	St*, IvIg*
13	2	SCLC	Hu	1/52	C, R, PE*
Painful form					
14	6	SCLC	Hu	1/46	R, C
15	6‡	Gastric (malignant lymphoma)	Hu	2/62	C
16	2	Gastric (adeno)	–	1/93	None
17	3	Non-SCLC (adeno-squamous cell)	–	1/46	None

*Effective treatment for neurologic symptoms.
†Primary lesion is unknown.
‡Although the cancer was diagnosed 3.5 years prior to the neurologic onset, she had remission after chemotherapy. Six months from the appearance of neuropathic symptoms, the recurrence of cancer was detected.
SCLC = small cell lung cancer; Hu = anti-Hu antibody; C = chemotherapy; R = radiation therapy; CV2 = anti-CV2 antibody; Ope = operation therapy; St = steroids therapy; IVIg = intravenous immunoglobulin therapy; PE = plasma exchange; – = absent.

was also reported, and Romberg sign was positive in 1 patient (Patient 15). Painful sensation was their main complaint and deep sensory disturbance was mild compared to that of patients in the former group. Therefore, we designated the former group as ataxic form and the latter group as painful form in this study.

As for the deep tendon reflexes, all ataxic form patients showed reduced or absent reflexes, while two of the painful form patients (Patients 16 and 17) showed preserved reflexes. Motor function was only partially assessed because the painful form patients proved difficult in examining the muscle strength due to pain, but 3 patients (Patients 15 to 17; 75%) showed mild muscle atrophy. A mild to moderate degree of muscle weakness was noted in 6 patients (Patients 5, 8 to 12; 46%) of the ataxic form, and one of these patients (Patient 9) showed fasciculation on the limbs. Autonomic symptoms were reported in 7 patients, 6 patients of the ataxic form and 1 patient of the painful form. Three patients including one patient of the painful form (Patients 1, 3, and 17) showed urinary retention and the other 3 patients (Patients 9, 10, and 12) showed constipation. One patient of the ataxic form (Patient 4) presented orthostatic hypotension.

In the ataxic form, small cell lung cancer was seen in 7 patients (54%), non-small cell lung cancer in 2 patients (15%), gastric adenocarcinoma in 2 patients (15%), small cell mediastinal cancer in 1 patient, and adenocarcinoma (primary lesion was unknown) in 1 patient (table 2). In the painful form, each patient developed a different cancer, including small cell lung cancer, gastric adenocarcinoma, gastric malignant lymphoma, and non-small cell lung cancer (table 2). Neurologic symptoms developed before the diagnosis of cancer in 15 patients. The mean interval between the onset of neurologic symptoms and cancer diagnosis was 6.9 ± 7.0 months in the ataxic form patients and 4.3 ± 2.1 months in the painful form patients. These observations suggest that there was no remarkable feature of cancer between the ataxic and painful form patients.

The treatments for cancer were performed using various combinations of operation, chemotherapy, and radiation in 14 patients (table 2).

Table 3 Nerve conduction study

	Median nerve									
	Motor			Sensory		Tibial nerve (motor)			Sural nerve	
	MCV (m/s)	DL (ms)	CMAP (mV)	SCV (m/s)	SNAP (uV)	MCV (m/s)	DL (ms)	CMAP (mV)	SCV (m/s)	SNAP (uV)
Ataxic form (n = 13)										
Range	46.7-59.1	3.1-5.2	4.8-12.0	29.4-58.0	0-9.3	34.0-43.0	3.2-5.9	3.6-11.3	24.6-51.0	0-6.0
Mean ± SD	51.2 ± 3.5	3.6 ± 0.6	8.7 ± 2.3	44.3 ± 9.4	2.6 ± 3.0	38.9 ± 2.8	4.6 ± 0.8	7.8 ± 2.6	36.5 ± 13.4	0.8 ± 1.8
Not elicited			None (0%)		4 cases (33%)			None (0%)		9 cases (75%)
Painful form (n = 4)										
Range	42.6-53.1	3.1-4.7	2.8-5.5	34.3-47.0	0-6.0	40.0-43.2	4.4-5.8	0.9-8.8	39.0-50.4	0-8.2
Mean ± SD	48.4 ± 4.3	4.1 ± 0.7	4.0 ± 1.3	39.2 ± 6.8	2.8 ± 2.5	41.5 ± 1.7	5.0 ± 0.7	3.4 ± 3.6	44.7 ± 8.1	4.6 ± 3.4
Not elicited			None (0%)		1 case (25%)			None (0%)		1 case (25%)
P Ataxic vs painful form	NS	NS	0.009	NS	NS	NS	NS	0.029	NS	0.04
Controls (n = 121-191)										
Mean ± SD	57.8 ± 3.7	3.4 ± 0.4	10.7 ± 3.5	57.8 ± 4.7	23.5 ± 8.4	46.9 ± 3.5	4.5 ± 0.8	10.9 ± 3.8	51.0 ± 5.1	11.5 ± 4.7

Statistical analyses were performed using Wilcoxon rank sum test. Control values are based on previous reports.[31, 33]
MCV = motor nerve conduction velocity; DL = distal latency; CMAP = compound muscle action potential;SCV = sensory nerve conduction velocity; SNAP = sensory nerve action potential; NS = not significant.

Although these treatments were effective to decrease the cancer in some cases, an improvement or stabilization of neurologic symptoms was reported only in 2 patients of the ataxic form (Patients 1 and 8). In 4 ataxic form patients, immunologic treatment, including IV immunoglobulin therapy (IVIg), plasma exchange, and corticosteroid therapy, was performed, and the neurologic symptoms improved slightly for a short period in 3 of the patients (Patients 5, 12, and 13). No immunologic treatment was performed in patients of the painful form.

In the examination for onconeural antibodies, anti-Hu antibody was found in 7 ataxic form patients (54%), and one of these patients also presented anti-CV2 antibody. Two painful form patients (50%) also showed anti-Hu antibody (table 2). The other onconeural antibodies assessed were not detected in any of the patients. The levels of CSF protein ranged from 40 mg/dL to 596 mg/dL, and all patients except for one (Patient 6) belonging to the ataxic form had an elevated CSF protein level over 45 mg/dL. The mean CSF protein level was 138.1 ± 176.0 mg/dL in the ataxic form and 61.8 ± 22.2 mg/dL in the painful form. Cell counts in the CSF were slightly elevated over 5 cells/mm^3 in 3 patients with the ataxic form.

Electrophysiologic and pathologic characteristics of the two groups. Nerve conduction studies revealed a severely decreased amplitude of sensory nerve action potentials (SNAPs) in the median and sural nerves. In the ataxic form, amplitudes of SNAPs in the sural nerves were less than that in the painful form ($p = 0.04$) (table 3). Sensory nerve conduction velocity (SCV), motor nerve conduction velocity (MCV), and distal latency were mildly prolonged in both forms. The compound muscle action potentials (CMAPs) were predominantly decreased in the patients with the painful form compared to that of the ataxic form patients ($p = 0.009$ for median nerve, $p = 0.029$ for sural nerve) (table 3).

In the sural nerve biopsies, a reduction of the myelinated fiber density was seen in all cases and in various degrees (329 to 5,751 fibers/mm^2) (table 4). Individual morphometric data of the sural nerve biopsy specimens are listed in table E-2. There was a marked difference in the proportion of small fiber and large fiber reduction between the two groups. Large myelinated fibers were severely depleted, while small myelinated fibers were mild to moderately decreased in most of the ataxic form patients (figure). The large myelinated fiber density was 336 ± 402 fibers/mm^2 (26 to 1,382 fibers/mm^2) and the small myelinated fiber density was 1,701 ± 1,445 fibers/mm^2 (237 to 4,922 fibers/mm^2), indicating that large myelinated fiber loss was the predominant feature in the ataxic form (table 4). On the other hand, the reduction of large myelinated fibers was significantly less ($p = 0.017$), while the reduction of small myelinated fibers was more, but not significantly, profound in the painful form patients compared to the ataxic form patients, although extensive variation was present (figure). The large myelinated fiber density was 1,426 ± 1,053 fibers/

Table 4 Pathology of the sural nerve

	MF density (fibers/mm^2)					Teased-fiber study (%)		
	Large	Small	Total	Small/large	UMF density (Fibers/mm^2)	Segmental de-/remyelination	Axonal degeneration	Sprouting of MF (n/mm^2)
Ataxic form (n=13)								
Range	26-1,382	237-4,922	329-5,054	2.46-93.12	7,251-34,875	0-27	8-85	0-131
Mean ± SD	336 ± 402	1,701 ± 1,445	2,037 ± 1,676	13.9 ± 25.6	18,045 ± 8,916	7.3 ± 9.0	54.6 ± 25.5	17.8 ± 35.3
Painful form (n=4)								
Range	296-2,461	138-3,290	434-5,751	0.44-1.34	213-12,865	0-4	22-72	0-33
Mean ± SD	1,426 ± 1,053	1,476 ± 1,505	2,902 ± 2,540	0.81 ± 0.43	7,150 ± 5,373	2.8 ± 1.9	46.5 ± 20.4	13.5 ± 14.2
P ataxic vs painful	0.017	NS	NS	ND	0.039	NS	NS	NS
Controls (n=9)								
Mean ± SD	3,068 ± 294	5,122 ± 438	8,190 ± 511	1.7 ± 0.2	29,913 ± 3,457	3.8 ± 2.2	0.5 ± 0.8	

Statistical analyses were performed using Wilcoxon rank sum test. Control values (mean ± SD) are based on previous reports.[25, 32]
MF = myelinated fiber; UMF = unmyelinated fiber; NS = not significant; ND = not determined.

mm^2 (296 to 2,461 fibers/mm^2) and the small myelinated fiber density was 1,476 ± 1,505 fibers/mm^2 (138 to 3,290 fibers/mm^2), indicating that small myelinated fiber loss, compared to that of large myelinated fibers, was the predominant feature in the painful form (table 4). Although there was a wide variation in unmyelinated fiber density (table E-2), the reduction was significantly more marked in the painful group than the ataxic group (7,150 ± 5,373 fibers/mm^2 vs 18,045 ± 8,916 fibers/mm^2, $p = 0.039$; table 4). Taken together, predominant small-fiber loss was the characteristic feature of the painful group. In teased-fiber preparations, the frequency of axonal degeneration was elevated in all patients (52.6 ± 24.0%), and these axonal features were indistinguishable between the two groups. In three patients (Patients 1, 2, and 12), the frequency of segmental de/remyelination was slightly elevated. No remarkable axonal sprouting or inflammatory change was observed in either group.

Figure Transverse section of a sural nerve specimen from control subject, ataxic form patient, and painful form patient

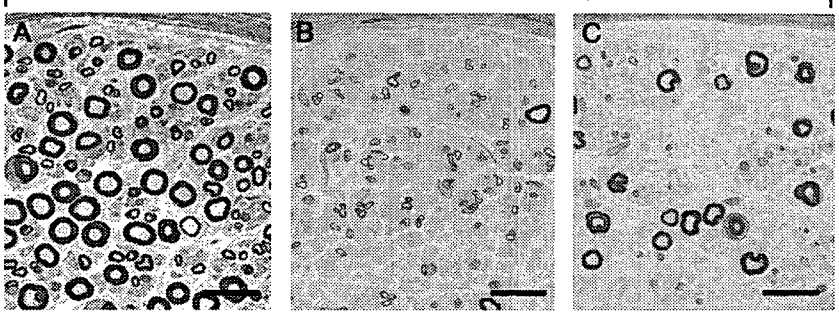

(A) Transverse section of a sural nerve specimen from a control subject. (B) Specimen from an ataxic form patient (Patient 7). Large myelinated fibers are severely depleted, while small myelinated fibers are mildly reduced. (C) Specimen from a painful form patient (Patient 14). In contrast to large myelinated fiber-predominant loss seen in B, large myelinated fibers are moderately preserved, while small myelinated fibers are severely reduced. No axonal sprouting is observed in B or C. Scale bar = 20 μm.

DISCUSSION The results of the present study clearly demonstrate that paraneoplastic neuropathy shows a wide variety of symptoms ranging from sensory ataxia to painful sensory impairments. In our series, approximately one fourth of consecutive patients showed predominantly painful sensation, while the rest were associated predominantly with sensory ataxia. The most well recognized form of paraneoplastic neuropathy is a sensory ataxic neuropathy characterized by profound impairment of kinesthetic sensation.[4,5,8] Only one patient showing small fiber neuropathy has been reported anecdotally,[34] while previous reports have indicated that paraneoplastic neuropathy is rather heterogeneous in its clinical manifestations.[7,16] A characteristic feature of our four painful form patients was predominant pain symptoms, particularly mechanical hyperalgesia associated with no or only a mild degree of sensory ataxic symptoms. In these patients, the nerve fiber loss was predominant in small myelinated and unmyelinated fibers, although large myelinated fibers were also decreased to some extent. In contrast, the ataxic form patients showed a loss of predominantly large myelinated fibers, confirming the previous pathologic findings of this type of neuropathy.[10,11] Electrophysiologic observations, particularly SNAPs, were relatively well preserved in the painful form patients as compared to those of the ataxic form patients, which supports this pathology that small fibers were involved predominantly in these painful forms of neuropathy. According to the classic symptoms of paraneoplastic syndromes proposed by Graus et